AN ABSTRACT OF THE THESIS OF

TERENCE RICHARD MATTOON for the degree of MASTER OF SCIENCE

in CHEMISTRY presented on July 24, 1981

Title: A THREE-PHASE ARGON PLASMA ARC FOR ANALYTICAL EMISSION SPECTROSCOPY

Abstract approved: Redacted for Privacy

Edward H. Piepmeier

A new three-phase argon plasma arc was developed for analytical emission spectroscopy. The power supplied to the plasma arc utilized a simple circuit with three-phase ac line voltage stepped down via a transformer to 104 V_{rms}. A three concentric quartz tubing assembly was determined to be the optimum configuration for supplying argon and sample aerosol to the plasma. A Babington-type nebulizer with a split sample aerosol flow stream was constructed and used to supply sample aerosol to the three-phase plasma arc. The three-phase argon plasma arc has an area of low electron density in the center which enabled the sample, in aerosol form, to be efficiently introduced into the plasma. Desolvation of the sample aerosol prior to reaching the plasma enhanced the emission signal by 30%. Detection limits between 0.1 ppm and 2 ppm were determined for seven elements. Calibration curves yielded a linear dynamic concentration range of approximately three orders of magnitude. Background emission from the tungsten electrodes employed was recorded from 250-600 nm.

A Three-Phase Argon Plasma Arc For Analytical Emission Spectroscopy

by

Terence Richard Mattoon

A THESIS

submitted to

Oregon State University

in partial fulfillment of
the requirements for the
degree of

Master of Science

Completed July 1981

Commencement June 1982

APPROVED:

Redacted for Privacy

Professor of Chemistry in charge of major

Redacted for Privacy

Chairman of Department of Chemistry

Redacted for Privacy

Dean of Graduate School

Date thesis is presented July 24, 1981

Typed by Renée Acquilano for Terence Richard Mattoon

TABLE OF CONTENTS

LIST OF FIGURES

LIST OF TABLES

A THREE-PHASE ARGON PLASMA ARC FOR ANALYTICAL EMISSION SPECTROSCOPY

INTRODUCTION

Emission spectrometry is a common analytical tool. In analytical emission spectroscopy a sample is excited by thermal or electrical energy, and the radiation emitted by the excited sample is measured and used for qualitative and quantitative analysis.

The excitation source, which thermally or electrically excites the sample, is very important in analytical emission spectrometry because of its influence upon both the pattern and intensity of lines emitted by the sample. The ideal excitation source for analytical emission spectrometry would include the following properties (1,2):

1) applicability to all states of matter
2) capability of exciting lines of a large number of elements
3) a wide dynamic concentration range
4) freedom from interferences
5) convenience of operation
6) low purchase, operation, and maintenance costs
7) high precision and detectability.

Excitation sources that have commonly been used for analytical emission spectrometry are flames, arcs, sparks, and plasmas.

In this thesis a new argon plasma arc using three-phase ac power will be described, along with its applicability to analytical emission spectrometry.

HISTORICAL

Introduction

The basic technique of analytical emission spectrometry as a quantitative method of analysis began its development about fifty years ago, with the use of a flame as an excitation source. Flame emission spectrometry was a commonly used analytical tool for many years. The flame, however, is limited in several ways as an excitation source. The low temperatures of the common flames, 1700-3500°K, limits the flames as far as the number of lines excited and detection limits. Also the composition of the flame lends itself to chemical interferences.

Higher temperatures can be achieved by introducing the sample into an electrical discharge, such as an arc or spark. Such excitation sources can be useful as a means of identifying and quantifying a large number of elements simultaneously in almost any matrix ranging from alloys, ores, ashes of organic materials, to atmospheric dust. There are some limitations to using an arc or spark as an excitation source. First, liquids are not handled well in an arc or spark. Next, C_2N_2 emission bands, due to the use of carbon electrodes and the presence of the atmosphere, and general background emission raise the threshhold of detection. Further, the nature of the electrical discharge is strongly affected by the makeup of the sample, so that accuracy is achieved only by matching the sample and standard very closely, which is not always possible.

A newer excitation source for analytical emission spectrometry is the argon plasma, which combines the docility of the flame with the

high temperatures obtained in the arc or spark electrical discharges. A plasma is an electrically neutral, ionized gas composed of ions, electrons, and neutral particles. Usually when an argon plasma is used for analytical emission spectrometry, a stream of flowing argon is ionized by the influence of a strong electrical field. In the past, electrical fields used for this purpose have included radio frequency, direct current, and microwave.

To generate an argon plasma a few seed electrons and ions are supplied to the argon via a Tesla coil or if electrodes are employed, via shorting the electrodes. The argon ions and electrons which interact with the electrical field accelerate and encounter resistance through collisions with argon atoms. Great heating and an avalanche of argon ions and electrons results. This process occurs almost instantaneously, creating the argon plasma.

The argon plasma excitation sources have an added advantage over other excitation sources because they do not introduce their own chemical interferences, and because under the proper conditions sample matrix effects are minimal. Other advantages of plasma excitation sources will be detailed in latter paragraphs as two individual types of argon plasmas are described.

The three-phase argon plasma arc described in this thesis has characteristics similar to the radio frequency or inductively coupled plasma (ICP), and the direct current plasma (DCP), so these plasmas will be described in some detail. The common microwave argon plasma will not be considered further as it does not have as high a power dissipation as the ICP or DCP; hence it has not found very broad

applications for analytical emission spectrometry of solutions, which require considerable power to desolvate and heat the solvent.

Inductively Coupled Plasma

The Radio Frequency or Inductively Coupled Plasma (ICP) generated at atmospheric pressure was first described by Reed (3,4) in 1961. Argon was determined to be the simplest gas in which to start and operate the discharge. Powders were introduced into the discharge for purposes of crystal growth. Reed discovered that the sample would vaporize completely sometimes, which suggested that this discharge could be used as an excitation source.

The analytical potentials of the ICP were revealed in papers by Greenfield (5) and Fassel (6) in 1964 and 1965 respectively. Some of the important studies that followed these were done by Wendt and Fassel (7), Greenfield et al. (8), Barnett et al. (9), Brisket et al. (10), Bordonal et al. (11), and Veillon and Margoshes (12). In 1969 Dickinson and Fassel (13) made some major improvements in the ICP, but it was not until 1974 that the first modern commercial ICP emission spectrometric instrument was introduced by Applied Research Laboratories (14,15). Presently there are several companies that market ICP units.

A more complete description of the ICP and its development can be found in review articles by Fassel (16) and Barnes (17). Recent developments in the ICP have been reviewed by Boyko et al. (18).

The ICP quartz torch assembly consists of three concentric quartz tubes through which argon flows at a total rate of approximately 20 L/min (see Figure 1). The argon flow inside the outer tube is

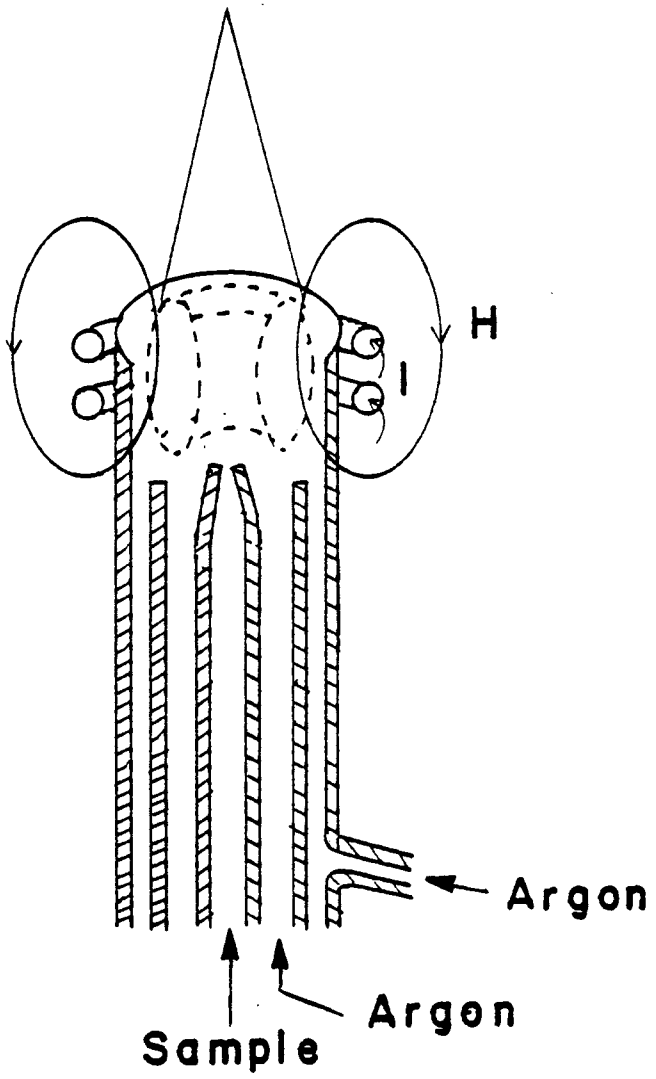

Figure 1. Inductively Coupled Plasma Source.

approximately 18 L/min. The flow rates inside the other two tubes are approximately 1 L/min each. The argon flow in the outer tube (25 mm i.d.) is so high because it cools the upper portion of the outside quartz tube as well as feeds the plasma. The purpose of the flow of argon through the middle tube (20 mm i.d.) is to lift the plasma away from the inner sample injection tube. The 1 L/min argon flow through the inner sample injection (1 mm i.d.) tube is for transport of the sample aerosol to the plasma. Surrounding the top of the quartz tube assembly is a water cooled induction coil, which is connected to a radio frequency generator.

The plasma is initiated by a spark from a Tesla coil. Once the gas ionizes and begins to conduct, the ions and electrons interact with the fluctuating magnetic field (H). At a radio frequency of 27 MHz the plasma forms into an annular shape, resulting in a hole or tunnel in the center of the plasma with a lower electron density. The sample aerosol is injected into this tunnel. Upon injection into the plasma, the sample aerosol is heated indirectly by radiation, convection, and conduction as it passes through this tunnel reaching 6000°K. The emission from the sample is viewed in the plume approximately 20 mm above the load coil, thus avoiding much of the background emission.

The ICP has many of the properties previously listed for an ideal excitation source. As for applicability to all states of matter, gases are the simplest to treat with a plasma. Examples of gases that have been introduced into a plasma are phosphine, metal hydrides, and ammonia (2). Methods for injecting powders into the ICP seem to suffer

due to differences in powder density and particle sizes, which result in segregation effects, agglomeration , and impacting of the powders (2). Separate vaporization of solids has been reported (19). Most all analyses done with the ICP are done with liquids which first pass through a nebulizer to produce an aerosol before being introduced into the plasma.

To compare other properties of the ICP with those of an ideal excitation source, I will begin with its high temperature (20), 6,000-10,000°C, which enables the excitation of numerous lines in a large number of elements. The dynamic range of the ICP has been reported up to 10^5-10^6 (21). Chemical interferences are minimal due to the high temperature, the absence of gases besides argon, and the longer residence time of the sample, which is twice the residence time of a sample in a typical flame. The precision of the ICP is good and the detection limits obtained with an ICP have been shown to rival the atomic absorption furnace for several elements (22). The ICP is convenient to operate and can be handled by technicians.

Some disadvantages of the ICP are the initial cost, and the cost of the high consumption of argon. Spectral interferences are a problem, since so many lines are excited. This problem is reduced by use of high resolution spectrometers. Another spectral problem is stray light. This problem is reduced by using either a double monochromator or a holographic grating in a monochromator , or both.

Direct Current Plasma

The first plasma arc devices intended for spectrochemical analysis were those described by Margoshes and Schribner (23) and Korolev and Vainshtein (24) in 1959. Both groups of workers used a plasma jet as their excitation source.

A plasma jet is a flow of partially ionized gas that is forced to stream out of a small orifice at high velocity. This gas stream has a flamelike appearance and usually derives its high temperature from a direct current discharge (25).

In these initial plasma arcs, a direct injector nebulizer was used to spray sample aerosol into the discharge between the cathode and anode. The observation region was in the current carrying portion of the plasma.

Numerous designs and modifications of the direct current plasma jet or plasma arc have been made in the past twenty years and have been reviewed by Keirs and Vickers (26) and Greenfield et al. (27).

The only commercially available DCP at the present writing is the Spectrometric Spectrospan III, as seen in Figure 2 (28). A plasma jet is formed between two spectrographic quality carbon anodes, which are at approximately a 60 degree angle to each other. The plasma is stabilized by a third tungsten electrode above the intersection of the two plasma jets. The result is an inverted Y-shaped plasma. The sample aerosol is injected below the plasma intersection near the anodes. Some of the droplets penetrate the plasma, but this is a region of high background emission so the emission observation is done just below the plasma intersection. The observation region is the

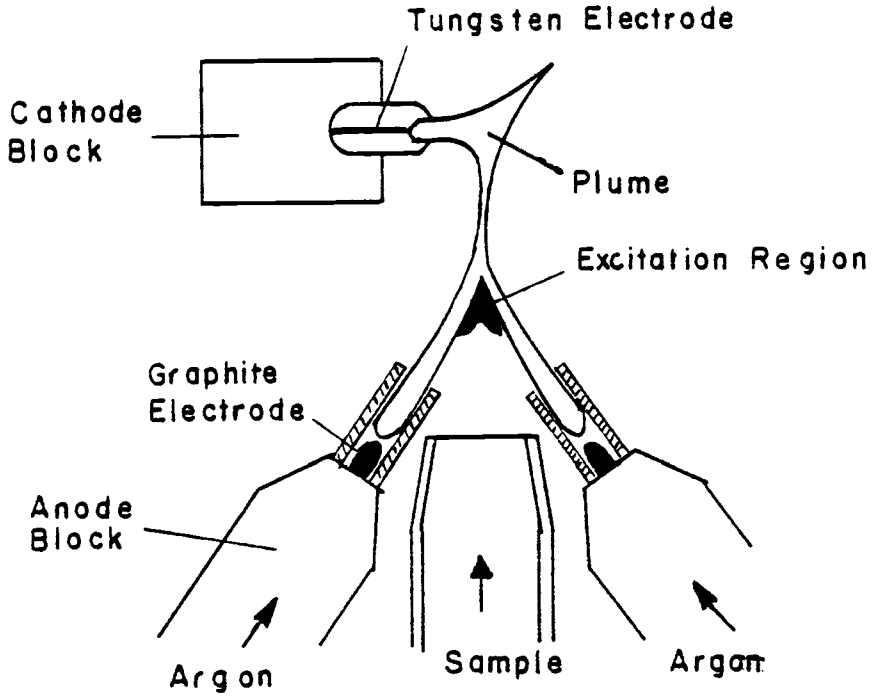

Figure 2. Direct Current Plasma Source.

same as the excitation region.

This direct current plasma (DCP) consumes about 9 L/min argon. Each anode requires 3 L/min of argon flow and the nebulizer also utilizes 3 L/min argon.

The current flow is 7 A dc at 117 V, resulting in a power dissipation of about 800 watts in the plasma. Temperatures have been reported between 6,000-10,000°K (29).

In the DCP a large portion of sample travels around the plasma and not through the plasma as it does in the ICP. By traveling around the plasma and not through it, some chemical interferents are not decomposed. Also, the sample that travels around the plasma into the cooler regions causes self absorption at higher concentrations. An advantage to a large portion of the sample traveling around the plasma is that more complex matrices can be introduced without extinguishing the plasma.

Detection limits obtained with a DCP have been uniformly poorer than detection limits obtained with an ICP (30). Since the detection limits set the lower limit of the dynamic range and self absorption sets the upper limit of the dynamic range, the DCP has a smaller dynamic range than the ICP. The reason self absorption is less of a problem in the ICP than the DCP is because the temperature across the plume of the ICP is essentially constant, and sample travels through the center of the ICP, thus reducing the probability of nonemitting sample in the cooler outermost region of the ICP.

The DCP has the advantage over the ICP in reduced cost of operation and simplicity. The consumption of argon and power in the DCP is

approximately half what is consumed in the ICP. The dc power supply for the DCP is much simpler than the radio frequency generator required for the ICP.

Three-Phase Plasma

The new three-phase argon plasma arc presented in this thesis was developed for several reasons. First, three-phase ac line voltage is readily available and a simple circuit can be used to control the power supplied to the argon plasma. Next, due to the alternating nature of three-phase ac a triangular shaped argon plasma can be formed with a hole in its center (similar to the ICP) that permits effective sample introduction into the plasma source and good thermal contact between the plasma and the sample to vaporize and atomize the sample. No other conventional form of power can produce a triangular shaped plasma. Also, this argon plasma excitation source was designed to consume less power than conventional argon plasma excitation sources and to operate at low argon flow rates, resulting in a lower operating cost than conventional argon plasma excitation sources.

Nebulizers

An important component of all emission spectrometers that use liquid or solution samples is the nebulizer. Typical nebulizers will be discussed as well as the nebulizer constructed for use with the new three-phase plasma arc.

Samples in solution form are the most common state of matter used for analysis in conjunction with a chemical flame or plasma. Solutions

are homogeneous samples, which are sometimes convenient to prepare. A nebulizer is a means of generating an aerosol from a solution. The aerosol is then introduced into the chemical flame or plasma for analysis.

A carrier gas is required for the formation of the aerosol and the transport of the aerosol from the nebulizer to the plasma. The flow rates of carrier gases used in conjunction with chemical flames is between 8 L/min and 20 L/min. The DCP utilizes a carrier gas flow rate of approximately 3 L/min and the ICP utilizes a carrier gas flow rate of approximately 1 L/min. The nebulizers used in conjunction with chemical flames at high carrier gas flow rates were too inefficient for aerosol production when used at the low flow rates required of the ICP. This prompted the modifications and new designs of nebulizers to be used with the ICP. Since the sample introduction into the new plasma arc described in this thesis is similar to the sample introduction in the ICP, a discussion of the types of nebulizers used in conjunction with the ICP will follow.

Three basic pneumatic nebulizer designs as well as ultrasonic nebulizers have been used with the ICP. The simplest design is that of the crossflow pneumatic nebulizer (see Figure 3), first described by Valente and Skrenk (31). The basic idea is that a stream of argon flowing through a glass capillary tube intersects at a right angle the sample solution stream which also has passed through a glass capillary tube. The result is the production of an aerosol. Both argon and sample orifices are 0.1 mm in diameter. The fact that the sample is required to pass through this 0.1 mm orifice leads to

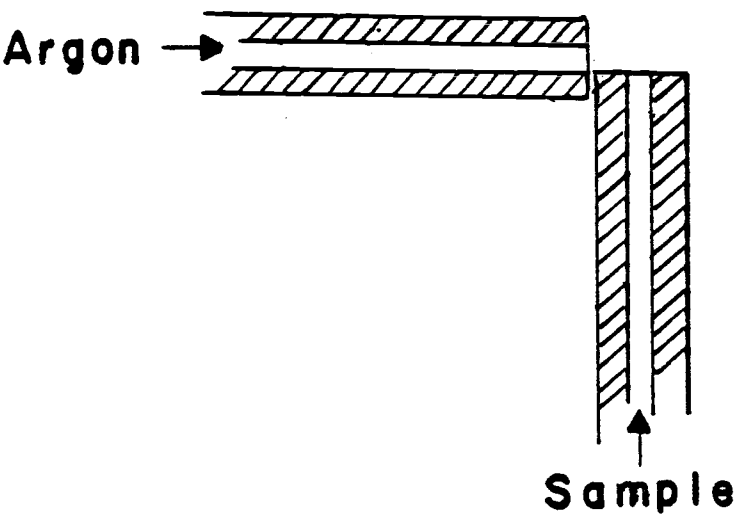

Figure 3. Crossflow pneumatic nebulizer.

a problem of clogging for sample solutions containing even very low amounts of solids. Another problem with this nebulizer is that the capillary tubes are easily misaligned, which results in a low nebulizer efficiency. This nebulizer design is currently used on some commercially available ICP units.

The second pneumatic nebulizer design to be considered is the Meinhard concentric tubes nebulizer, as seen in Figure 4 (32). The glass capillary tubes are configured so that argon passing through the external tube intersects with the sample at the exit forming an aerosol. This aerosol production is further enhanced by the placement of a glass bead impactor near the exit. An advantage to this nebulizer design is that the misalignment problem is eliminated. The sample solution passes through a 0.1-mm i.d. capillary tube, so the clogging problem associated with the cross flow nebulizer is also present in this nebulizer. The Meinhard concentric tubes nebulizer is also used on some commercially available ICP units.

The last pneumatic nebulizer design to be discussed is based on the Babington principle (33, 34). This principle involves the flowing of a film of the sample solution over the outside surface of a hollow glass or metal sphere which has a small orifice in the side. A gas under pressure flows out of this orifice resulting in the production of an aerosol. The aerosol production is enhanced by the placement of a glass bead impactor next to the orifice. A disadvantage to this design is that a lot of solution is wasted.

A modified Babington type nebulizer was developed by Fry and Denton (35, 36) for use with an atomic absorption instrument. The

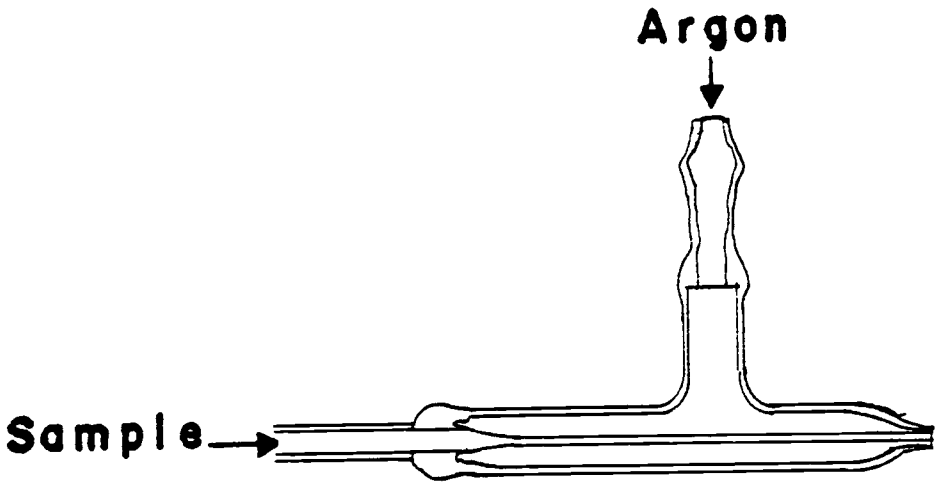

Figure 4. Meinhard concentric tubes pneumatic nebulizer.

first modified Babington-type nebulizers to be used in conjunction with ICPs were developed by Suddensorf and Bayer (37) and Wolcott and Sobel (38). They used a slot/orifice rather than a Babington sphere. Recently, modified Babington-type nebulizers using a Babington sphere (see Figure 5) have been used with ICPs (39) and a DCP (40).

An advantage of the modified Babington-type nebulizer is that solutions with high solids content can be nebulized, since the sample solution flows through a large orifice and only the gas flows through a 0.1-mm orifice. This nebulizer is easily adjusted. A modified Babington-type nebulizer is not commercially available.

The use of an ultrasonic nebulizer in conjuction with an ICP has been reported by several workers (5,13,41). The best results using an ultrasonic nebulizer with an ICP have been reported by Olson, Hass Jr., and Fassel (18). Their ultrasonic nebulizer consisted of the sample solution flowing over a borosilicate glass cylinder that was acoustically coupled with a transducer, operated at a 1.45 MHz (see Figure 6). An advantage of this type of nebulizer is the aerosol production is dependent on the frequency of the transducer only, not the argon flow rate. The ultrasonic nebulizer produces a uniform and small droplet size as much as ten times as dense as the aerosol produced in a pneumatic nebulizer. The detection limits reported with an ICP using an ultrasonic nebulizer were at least an order of magnitude better than those reported for pneumatic nebulizers. Ultrasonic nebulizers are commercially available, but are expensive and are more difficult to use than pneumatic nebulizers. Ultrasonic nebulizers are usually employed only when lower detection limits are required.

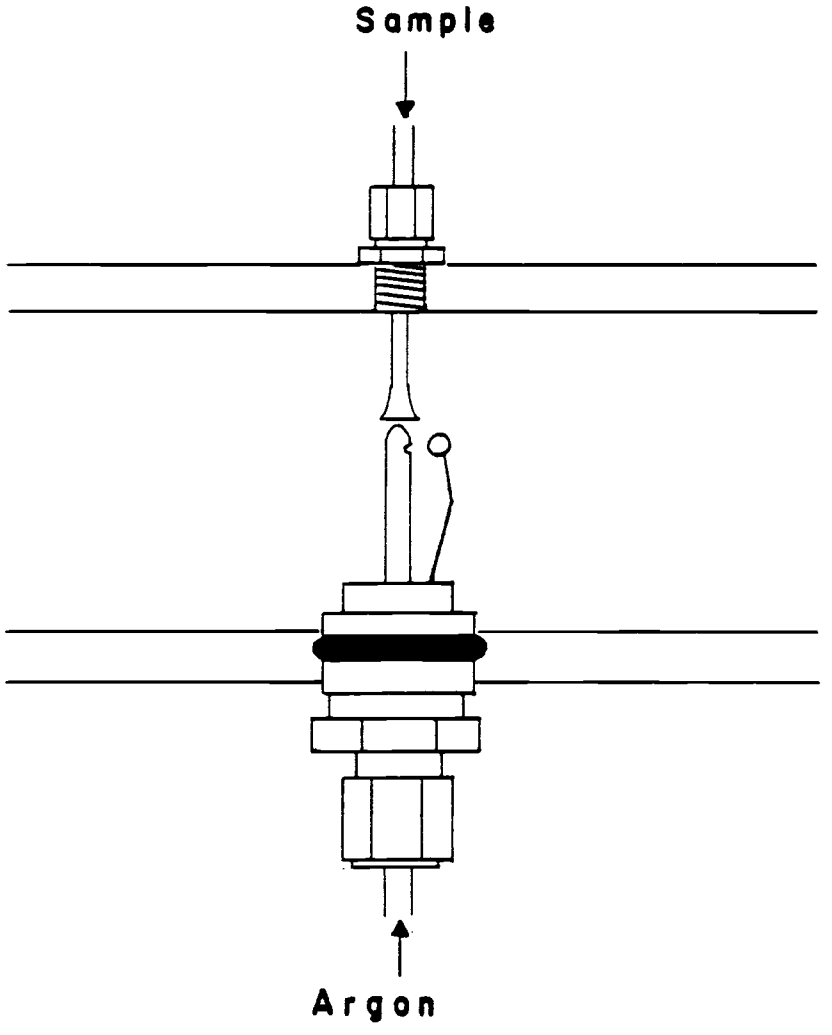

Figure 5. Modified Babington-type pneumatic nebulizer.

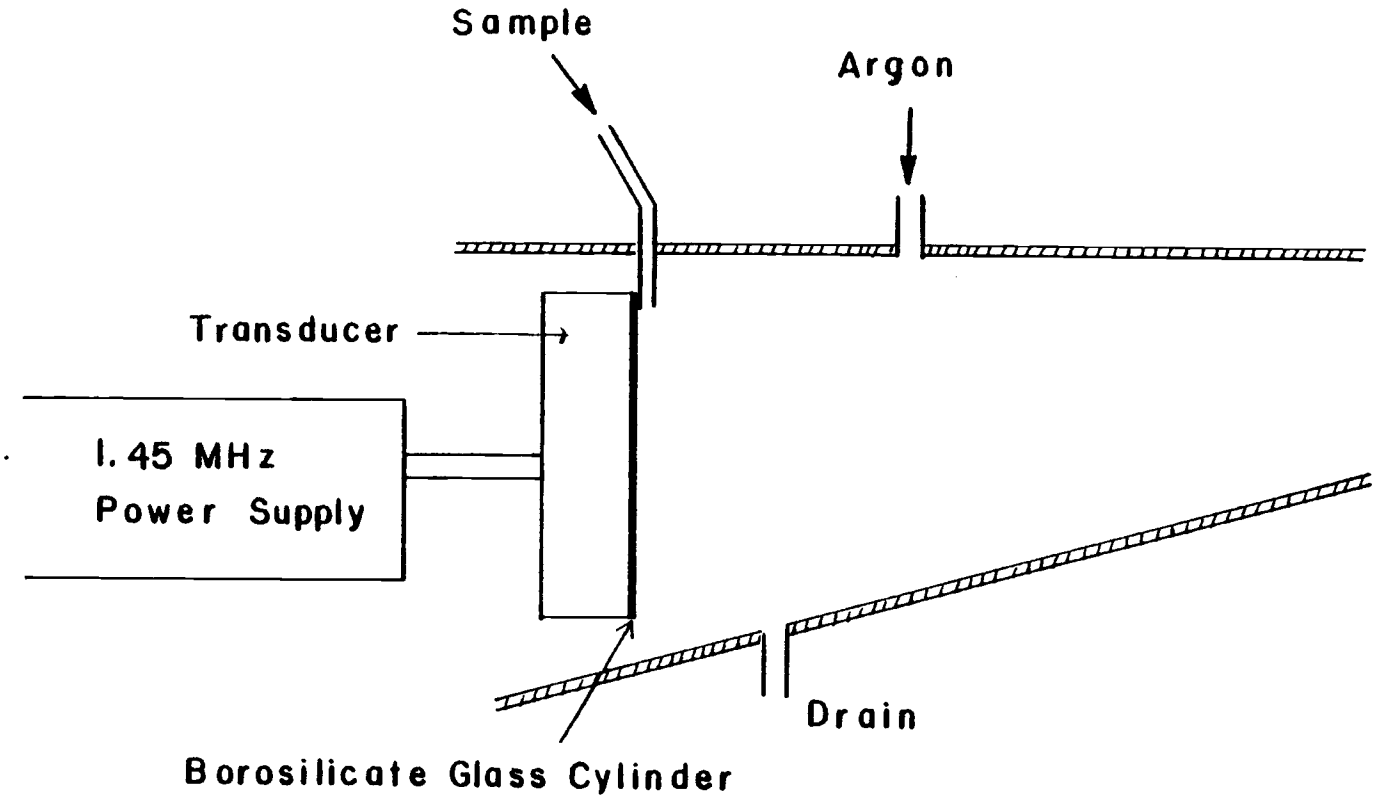

Figure 6. Ultrasonic nebulizer.

The nebulizer constructed for use with the three-phase plasma arc was based on the modified Babington nebulizer designs. The reasons for choosing this design were (1) construction is relatively easy, (2) samples could be nebulized without clogging, (3) adjustments of the nebulizer are easy, and (4) there are no misalignment problems.

INSTRUMENTATION

Electronics

The power used to sustain the argon plasma arc described in this thesis was derived from three-phase ac line voltage. Three-phase ac line voltage consists of three sine waves 120 degrees out of phase from each other (see Figure 7). Three-phase ac line voltage is transmitted through four wires with one wire corresponding to each phase and the fourth wire serving as a common. The voltage between any two of the three phases is 208 V_{rms} (root mean squared). This voltage was too large to be used with the argon plasma arc, so a transformer was used to step the voltage down to 104 V_{rms}.

A plasma arc operated at atmospheric pressure at low voltages and medium current has an essentially constant voltage drop across it for different current flows (42). This means that if the current supplied to the plasma arc is controlled, then the power dissipated in the plasma arc will also be controlled. Therefore, a circuit was developed to control and vary the sinusoidal current supplied to the plasma arc. Bipolar junction transistors were used as the electronic devices to control the current because of their small size, relatively low cost, and the simplicity of the total circuit in which the junction transistors were utilized.

The original idea was to use PNP junction transistors to control the current flow to the plasma arc and NPN junction transistors to control the current flow from the plasma arc. This was decided to be unnecessary since the total current flow into the plasma must equal the

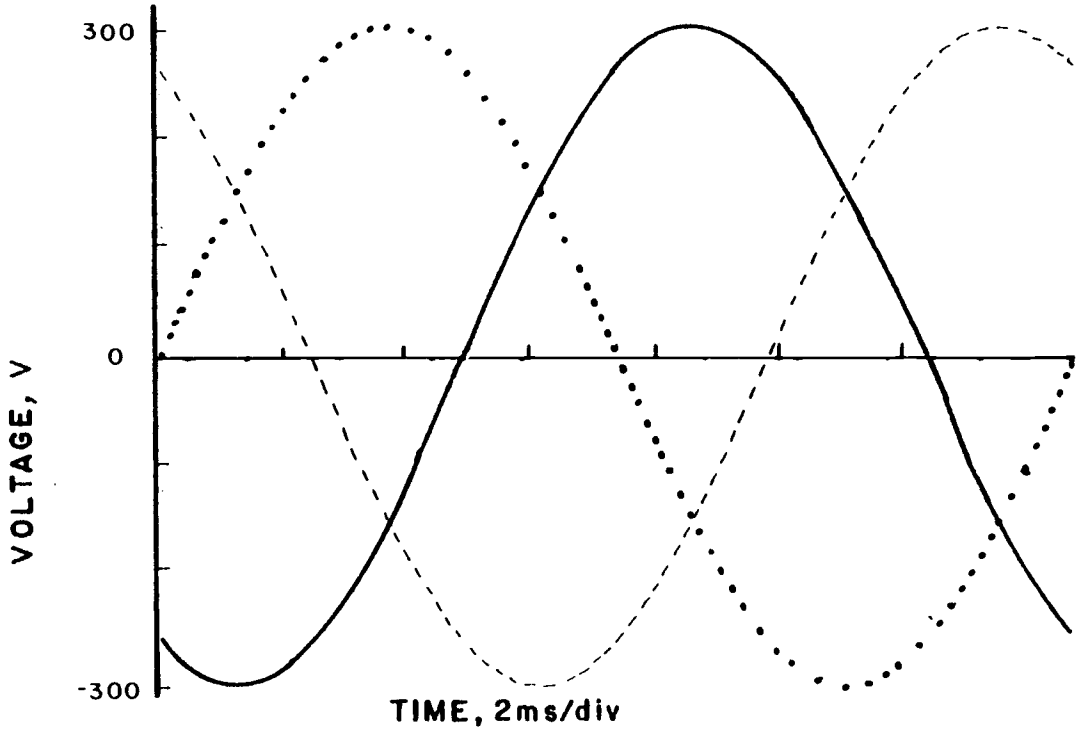

Figure 7. Three-Phase ac line voltage waveforms

total current flow out of the plasma, so by controlling either the current flow to or the current flow from the plasma the opposite will also be controlled. Since NPN transistors are more common than PNP transistors, it was decided to use NPN transistors to control the current from the plasma.

A circuit was devised to control the current on each of the three phases (see Figure 8). Therefore, there were three identical circuits each employing a NPN transistor, one for each electrode. From the diagram it can be seen that the circuit branches, and one section is half-wave rectified positively via a diode, D1, and the other section is half-wave rectified negatively via another diode, D2. The NPN transistor is on the negatively half-wave rectified section. The 3-Ω resistor, R2, Figure 8, serves to dissipate some of the power that would otherwise have to be dissipated by the transistor, and also serves to limit the maximum current flow through the circuit. The 3-Ω resistor is a 2-Ω, 200-watt resistor in series with two parallel 2-Ω, 200-watt resistors. The two parallel 2-Ω, 200-watt resistors, are equivalent to a 1-Ω, 400-watt resistor. The diode, D3, on the emitter side of the transistor prevents reverse biasing of the emitter-base junction on the transistor. The meters displayed average dc current.

The variable resistor R1, Figure 8, between the base of the transistor and the transformer common determines the current flow into the base from the transformer common as a function of base voltage, which follows within less than one volt of the emitter voltage. The current flow through the base multiplied by the current gain (h_{fe}) of

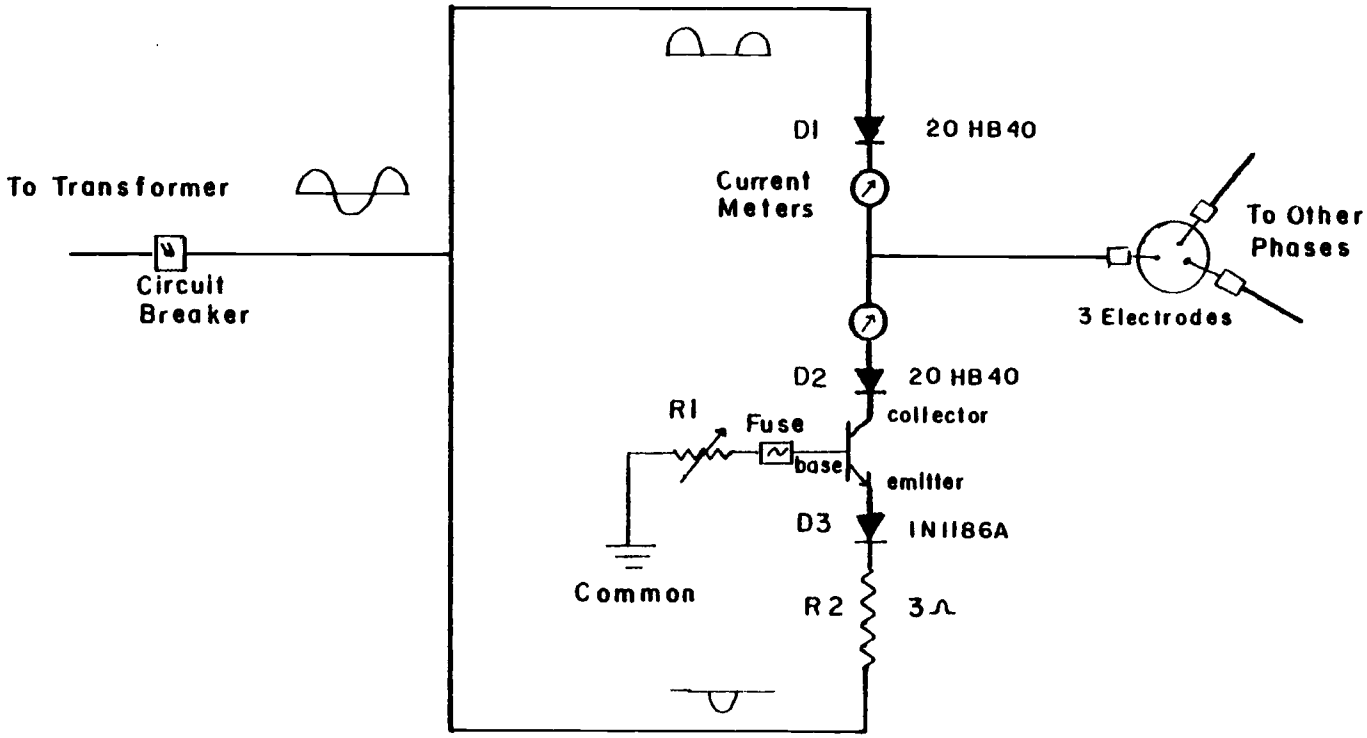

Figure 8. Circuit to control current with transistors.

the transistor gives the collector-emitter current (I_{CE}). By varying the size of the resistor, R1, Figure 8, between the base and common, the I_{CE}, which is the average current through the plasma arc, could be controlled.

Transistors used in this circuit, Figure 8, were required to operate at high currents, about 10 A, and have a collector-emitter breakdown voltage larger than the peak voltage from the transformer of 147 V. Operating at high currents and high voltages would also require a transistor with a high power dissipation rating. In view of these requirements along with the low cost requirement, a MJ10021 (Motorola) transistor was employed. The basic ratings of the MJ10021 transistor are listed in Table 1.

TABLE 1. MJ10021 TRANSISTOR RATINGS

Case Type	TO-3
Derate	1.4 W/°C
Current Gain (h_{fe})	75-1000
Maximum Power Dissipation	250 W
Maximum Base Current	20 A
Maximum Collector Current	60 A
Collector-Emitter Breakdown Voltage	200 V

For power dissipation the MJ10021 transistors were mounted on aluminum fin heat sinks with a derate of 0.8 W/°C. Three fans blowing approximately 60 ft^3/min each were used to blow air directly on each

transistor.

Three MJ10021 transistors were tested in the circuit shown in Figure 8. The transistors worked properly for several minutes, but then failed with the collector-emitter becoming an open circuit.

The operating conditions under which the transistors failed were monitored and will be presented along with a possible explanation of why the MJ10021 transistors failed in this circuit, Figure 8.

Voltage waveforms across the collector-emitter of the transistors were obtained using an oscilloscope. To obtain the voltage waveforms a Tektronix 555 Dual-Beam Oscilloscope was used with the following setting:

Time-Base	5 ms/cm
Source	line
Sweep Function	normal
Horz. Display	X1
Mode	add
Input 1	X10 probe connected to emitter 2 volts/cm Invert (pulled out)
Input 2	X10 probe to collector 2 volts/cm Invert (pushed in)

grounds on probes connected to each other.

Waveforms of the voltage across the collector-emitter (V_{CE}) across all three transistors using two different base resistors can be seen in Figure 9. The V_{CE} waveforms corresponding to the 50-kΩ base resistor and the 220- Ω base are substantially different, so will be discussed separately.

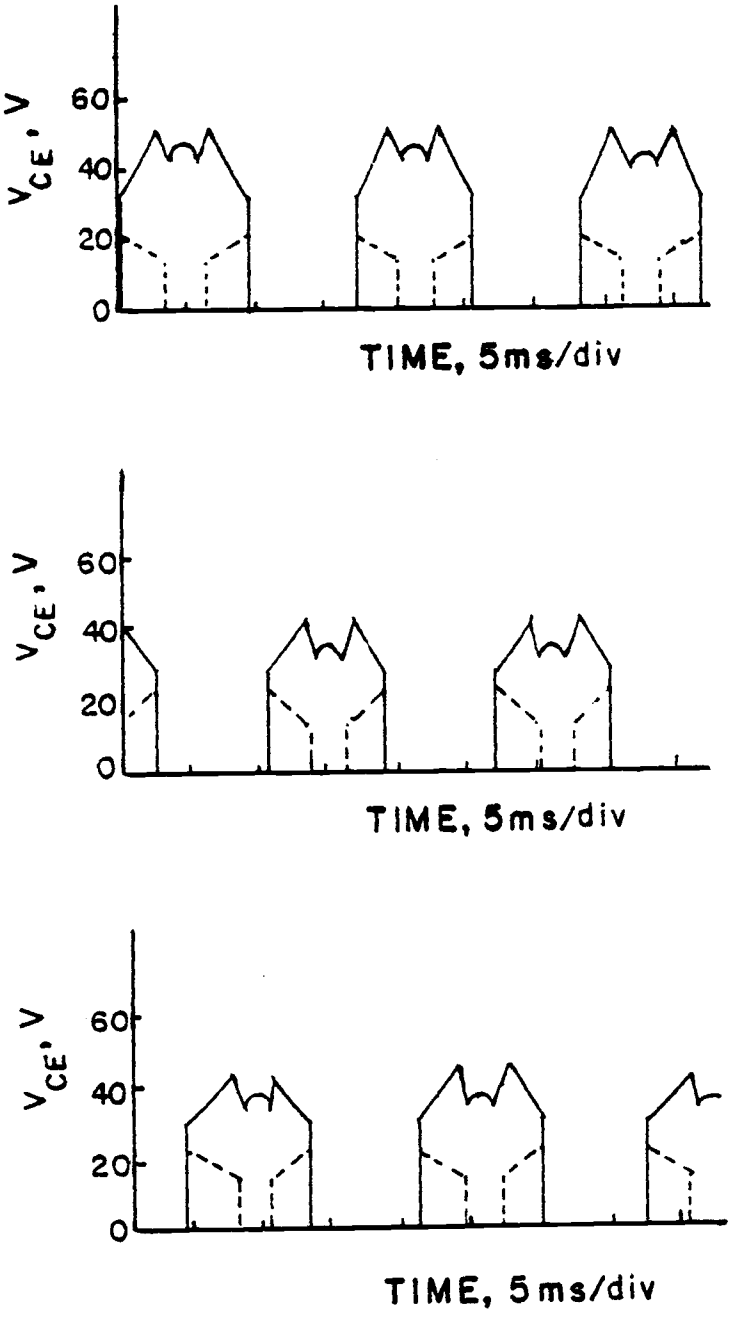

Figure 9. V_{CE} waveforms for a) transistor A b) transistor B c) transistor C

------ 220-Ω base resistor

——— 50-KΩ base resistor

To aid in the explanation of the V_{CE} waveforms, Figure 9, the V_{CE} waveform for transistor C corresponding to the 220-kΩ base resistor was redrawn, Figure 10a, next to an inverted three-phase ac line voltage waveform, Figure 10b. The V_{CE} waveform for transistor C corresponding to the 50-kΩ base resistor was also redrawn, Figure 11a, next to an inverted three-phase ac line voltage waveform, Figure 11b. Experimentally the phases A, B, and C, Figure 10b and 11b, were connected to the identical circuits A, B, and C, respectively, Figure 12. Transistors A, B, and C are the transistors in circuit A, B, and C, Figure 12, respectively. Since the bases of the transistors are connected to common, the amount of current flowing through a transistor is inversely proportional to size of the base resistor and proportionate to the negative phase voltage. The transistor automatically adjusts V_{CE} to cause the plasma electrode voltage to be whatever value is necessary to produce that current through the plasma.

The V_{CE} waveforms corresponding to the 220-Ω base resistor, Figure 10a, will now be discussed qualitatively. Prior to t_1', transistor C is reversed biased and the reversed bias voltage is dropped across the diodes D2 and D3, Figure 8, so the V_{CE} for transistor C is zero, Figure 10a. The current flow prior to t_1' is from circuit B to circuit A, Figure 12.

At time t_1', Figure 10a, transistor C has started to turn on and a small current is flowing through transistor C from circuit B, Figure 13. Current is still flowing between circuit B and circuit A, Figure 13. The current flow through transistor C is small at t_1',

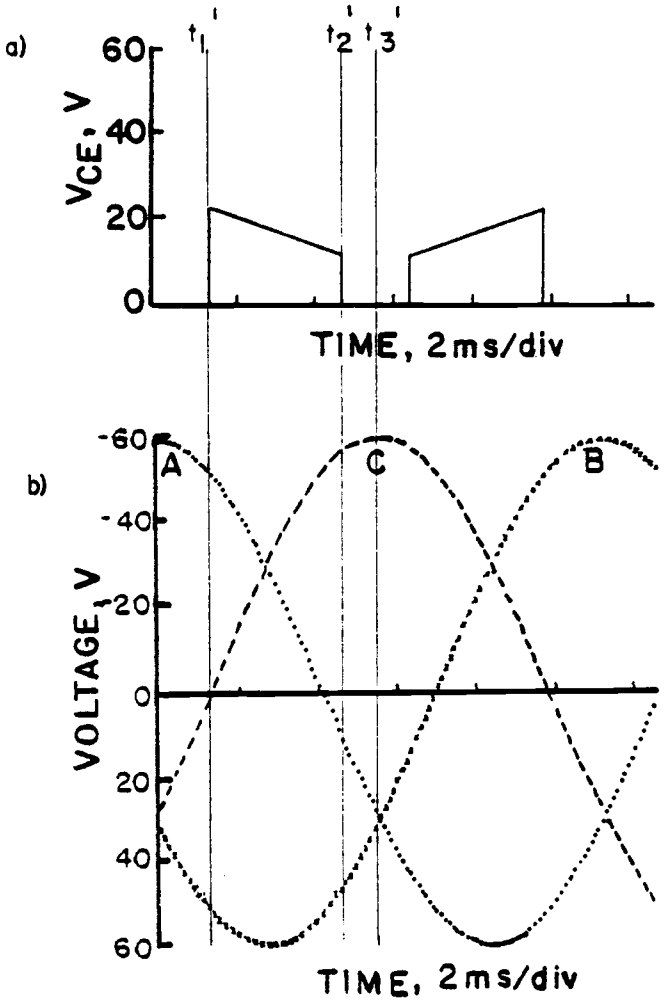

Figure 10. Voltage waveforms
a) V_{CE} across transistor C with 220-Ω base resistor
b) inverted three-phase ac line voltage

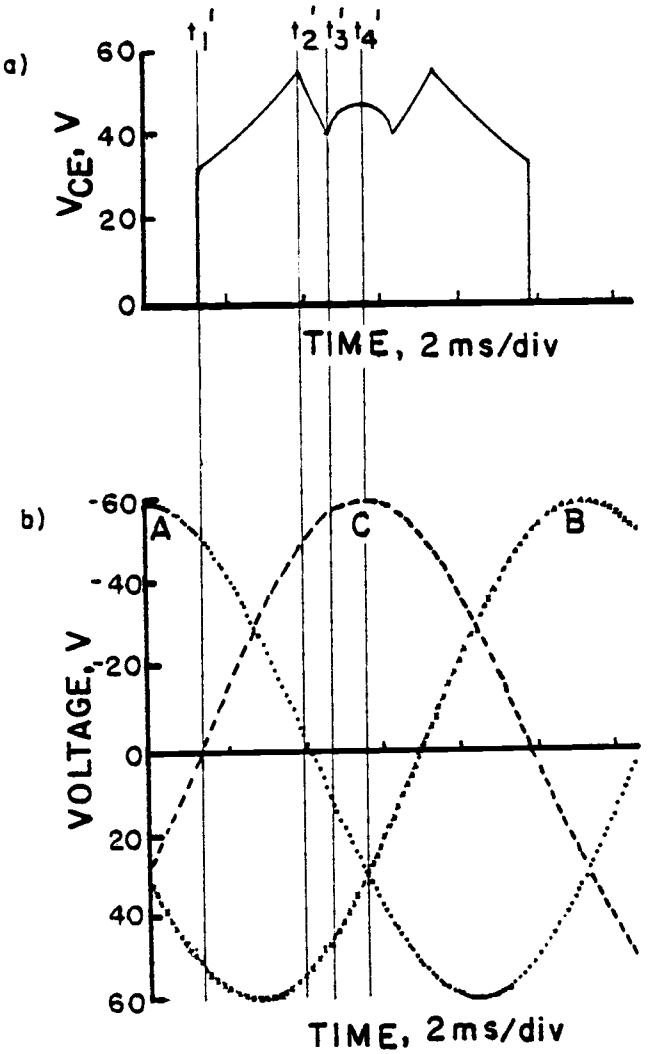

Figure 11. Voltage waveforms
a) V_{CE} across transistor C with 50-kΩ base resistor
b) inverted three-phase ac line voltage

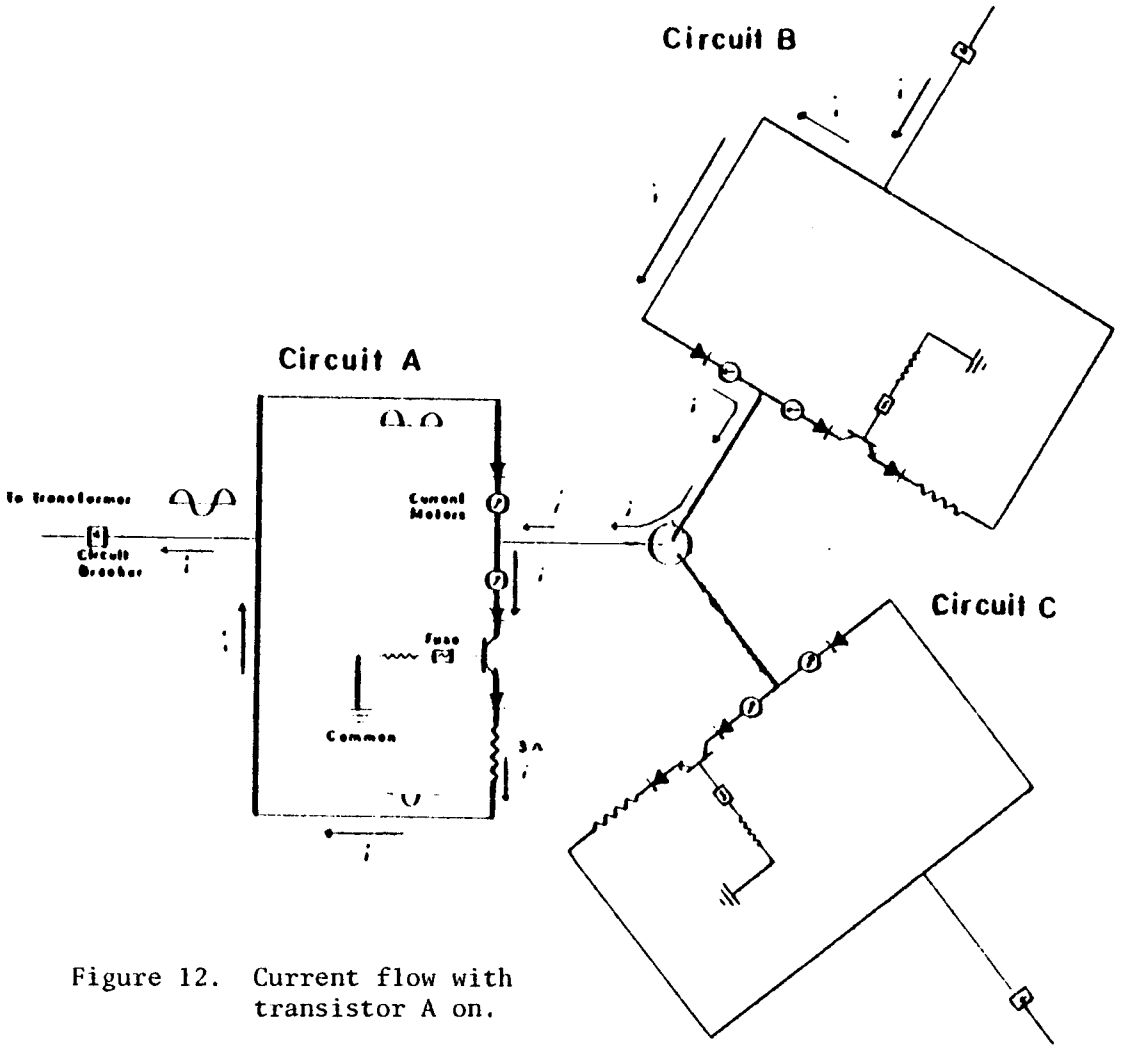

Figure 12. Current flow with transistor A on.

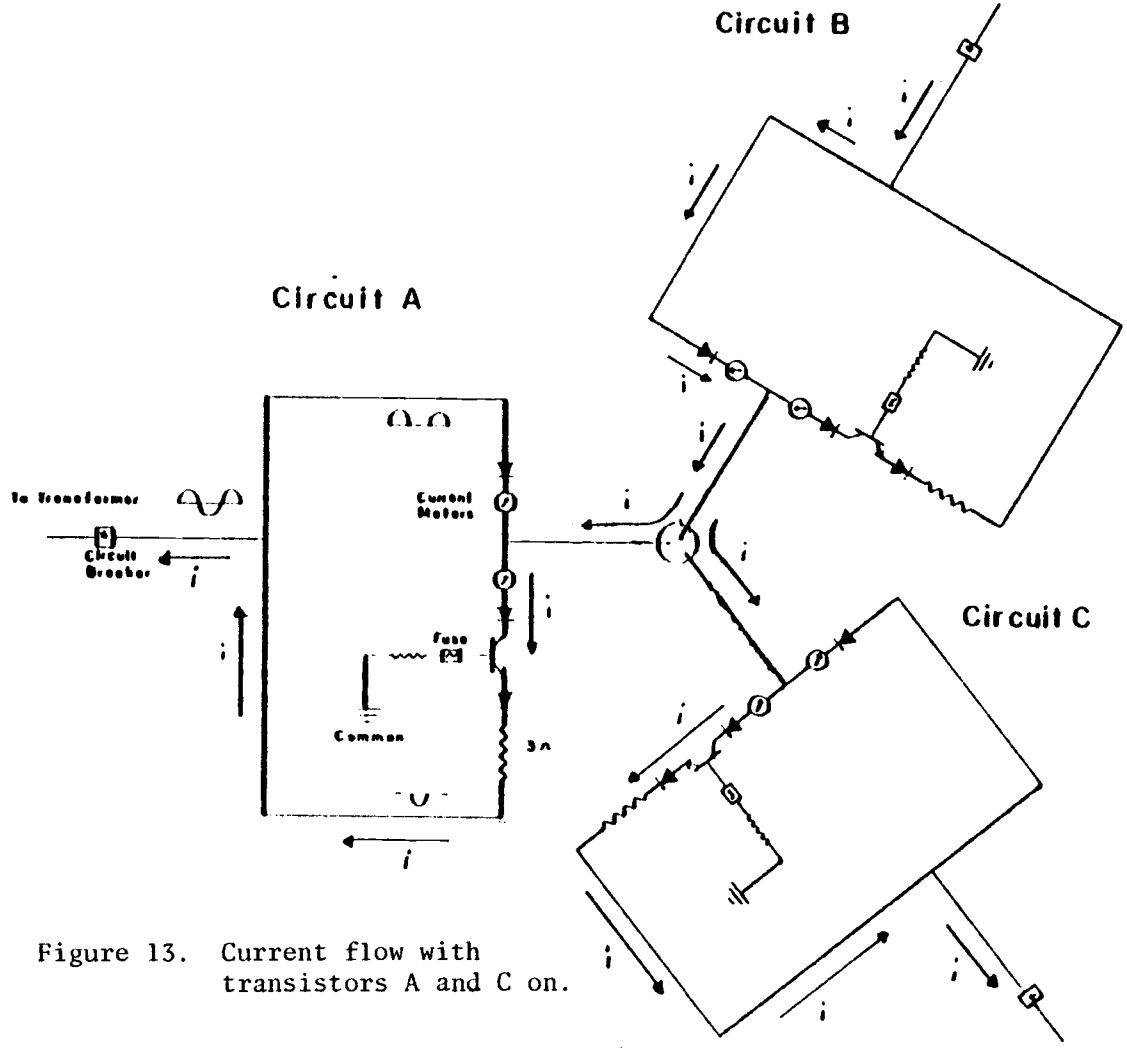

Figure 13. Current flow with transistors A and C on.

Figure 10a, so the voltage drop across the plasma need not be large. The rest of the voltage between phase B and phase C, Figure 10b, is dropped across transistor C.

During the time interval t_1' to t_2', Figure 10a, the current through transistor C is increasing because the phase C voltage is becoming more negative, Figure 10b. The transistor is turning on faster than the voltage is increasing between phase B and phase C, Figure 10b, so a decrease in V_{CE} across transistor C is seen between t_1' and t_2', Figure 10a.

During the time interval t_2' to t_3', Figure 10a, the current is flowing from circuit A and B to circuit C, Figure 14. There is no V_{CE} across transistor C, Figure 10a, which indicates it is fully turned on. There is no current control when a transistor is fully turned on, so with a 220-Ω base resistor the current was only controlled two-thirds of the time.

The C transistor V_{CE} waveform corresponding to a 50-kΩ base resistor is shown in Figure 11a. Prior to t_1', Figure 11a, the V_{CE} is zero for the same reasons previously discussed for the time prior to t_1', Figure 10a.

During the interval t_1' to t_2' the V_{CE} is increasing, Figure 11a, whereas the V_{CE} was decreasing in Figure 10a. The reason the voltage is increasing when the larger base resistor (50-kΩ) is employed is because the transistor is not turning on as hard or as fast as with the smaller base resistor (220-Ω). The current flow is from circuit B to circuit A and circuit C, Figure 13.

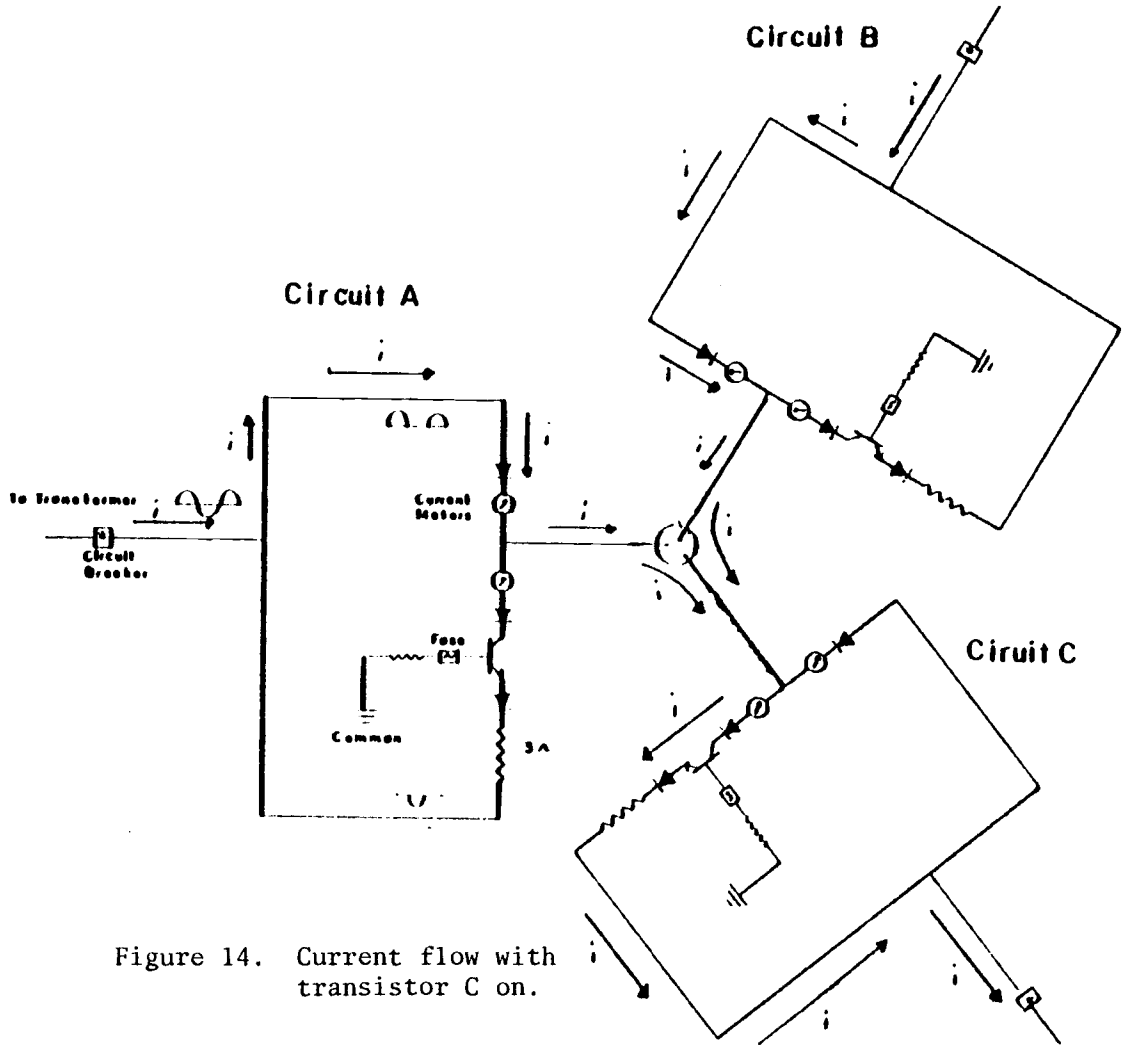

Figure 14. Current flow with transistor C on.

Between t_2' and t_3', Figure 11a, current flow is from circuit A and B to Circuit C, Figure 14. The voltage between phase B and phase C is essentially constant during t_2' to t_3', Figure 11b, yet transistor C is turning on harder as the plasma adjusts itself, so a decrease in V_{CE} is seen, Figure 11a.

During t_3' to t_4', Figure 11a, the current flow through transistor C is no longer increasing because the phase C voltage is essentially constant, Figure 11b. The V_{CE} is increasing slightly between t_3' and t_4', Figure 11a, as the plasma continues to adjust to voltage changes at electrodes A and B.

The last half of the V_{CE} waveform, Figure 11a, can be explained by reversing the above discussion. The transistors controlled the current all the time they were on, Figure 11a, when they were used with a 50-kΩ base resistor.

The important information extracted from the V_{CE} waveforms is that there is a substantial amount of voltage dropped across the transistor even when there was no control for one-third of the time they were on. Assuming the transistors are used to control the current all the time they are on, a large voltage will result.

The current meters in Figure 8 responded to average dc current. The current waveform should be sinusoidal in nature because the phase voltage is sinusoidal. The standard sinusoidal average to RMS current conversion can be used:

$$I_{rms} = 0.707/0.637\ (I_{ave}) \qquad (1)$$

The average current through the collector-emitter, I_{CE}, when the transistor failed was 7.6 A. So I_{rms} can be calculated from Equation (1):

$$I_{rms} = 0.707/0.637 \text{ (7.6 A ave dc)}$$

$$I_{rms} = 8.5 \text{ A}$$

An approximation of the base current was made by dividing the I_{CE} by the current gain (h_{fe}) of the transistor, thus; the base current was about 0.068 A.

The RMS V_{CE} was approximated from the waveforms V_{CE} to be 20 V_{rms}. An approximation of the power dissipated by the transistor would be:

$$P = V_{rms} \; I_{rms} \tag{2}$$

$$P = 20 \; V_{rms} \; (8.5 \; A_{rms})$$

$$P = 170 \text{ W}$$

In Table 2 a list of the rating of the MJ10021 transistor and the actual operating conditions under which the MJ10021 transistor failed are compared.

TABLE 2. COMPARISON OF MJ10021 TRANSISTOR RATINGS AND ACTUAL OPERATING CONDITIONS

Characteristics	Rating	Operating Condition
Max. Collector-Emitter Voltage	200 V	60 V
Max. Base Current	20 A	0.068 A
Max. Collector Current	60 A	8.5 A
Max. Power Dissipation	250 W	170 W

From Table 2 the only operating condition close to the rating of the transistor was power dissipation. This would indicate that the power dissipated by the transistor, although not above its rating, was excessive. This is reasonable because the maximum power dissipation of a transistor requires very efficient heat sinks and cooling systems. Apparently the cooling system used was not sufficient to dissipate the heat from the transistors, causing them to fail. The fact that the transistor took several minutes to fail would also suggest a heat build up problem.

The simple circuit shown in Figure 15 was then developed to provide current to the plasma. By changing the size of the resistors, the current is changed. This circuit worked successfully and was used for all the experiments in this thesis.

The calculation of the power dissipation in the plasma is dependent on the configuration of both the transformer and the load. The transformer is in a wye configuration and the load or plasma is in a delta configuration. The equation for the total power (P_T) base or a wye configured transformer and a delta load, assuming all three phases are identical and sinusoidal is (43):

$$P_T = 3V_L I_p \cos\phi_p \tag{3}$$

where V_L = line voltage

I_p = phase current

ϕ_p = power factor angle.

The line voltage (V_L) was measured as the voltage drop between two electrodes in the plasma. The phase current (I_p) is the current flow

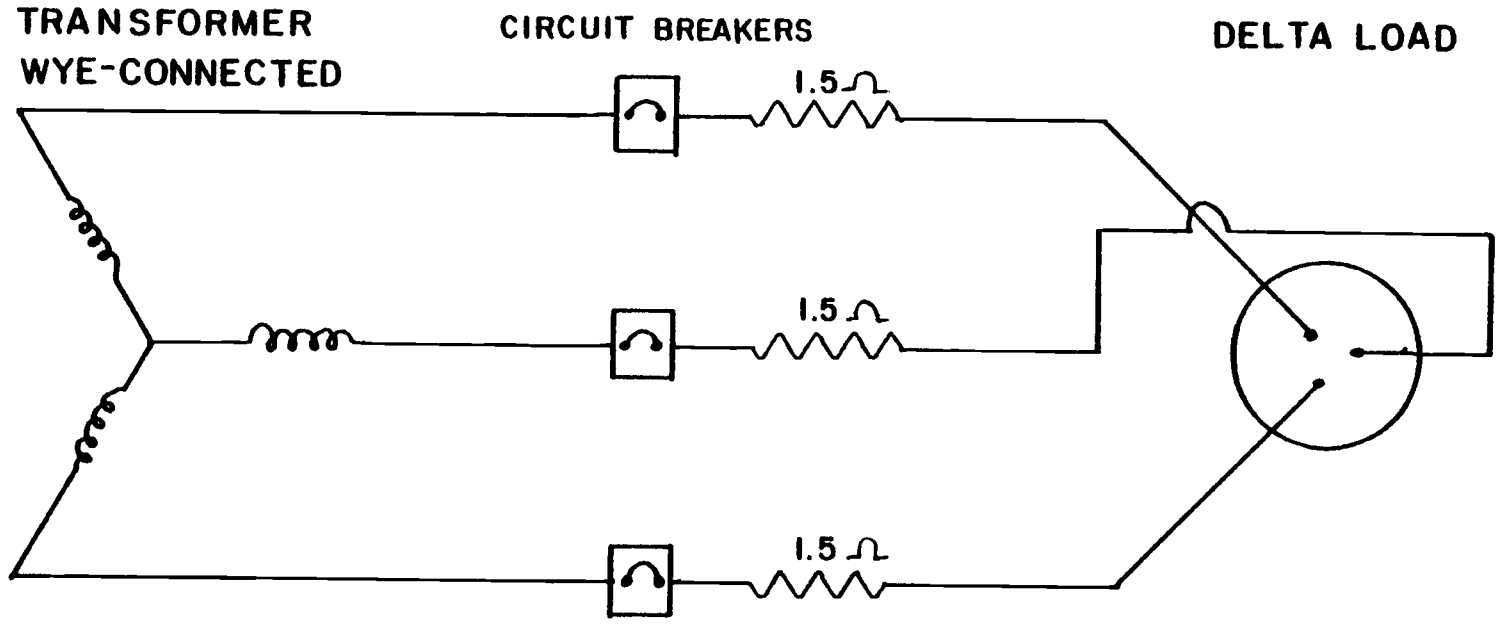

Figure 15. Simple circuit to control current to plasma.

through one phase. The power factor angle is the phase angle between current and voltage, which with my circuit was zero. Since the power factor angle is zero, cos ϕ_p goes to one and Equation (1) can be rewritten as:

$$P_T = 3\ V_L I_p \tag{4}$$

The current waveforms observed across the 1.5-Ω resistors appeared to be sinusoidal. Voltage waveforms obtained between two electrodes in the plasma are shown in Figure 16. The voltage waveforms in Figure 16 are approximately sinusoidal. This means an estimate of the voltage drop between two electrodes can be measured via a meter responding to sinusoidal voltage waveforms.

The Fluke 8020A Multimeter responds to sinusoidal voltage waveforms, so was used to measure the voltage drop between two electrodes. The root mean squared voltage obtained was 11 V.

The ac phase current was measured with an ac current meter to be 24 A average ac for each phase. This corresponds to 12 A average dc. To calculate power the RMS current is required. The conversion factor for average current to RMS current is:

$$I_{rms} = 0.707/0.637\ (I_{ave}) \tag{1}$$

The RMS current for each phase is:

$$I_{rms} = 0.707/0.637\ (12\ A_{ave}\ dc)$$

$$I_{rms} = 13\ A_{rms}\ dc$$

The total power can now be calculated from equation (3):

$$P_T = 3(11\ V_{rms})\ 13\ A_{rms}\ dc$$

$$P_T = 430\ W$$

The total power dissipated in the plasma arc is approximately 430 watts.

The 430 watts supplied to the plasma was the maximum power this circuit, Figure 15, could supply to the plasma. This is because higher power supplied to the plasma results in higher power dissipated by the resistors in the circuit, which the resistors could not tolerate. The approximately 430 watts of power dissipated in the three-phase plasma arc is close to one-half the approximately 800 watts dissipated in the DCP, and less than one-half the 1.0 kilowatts dissipated in the ICP.

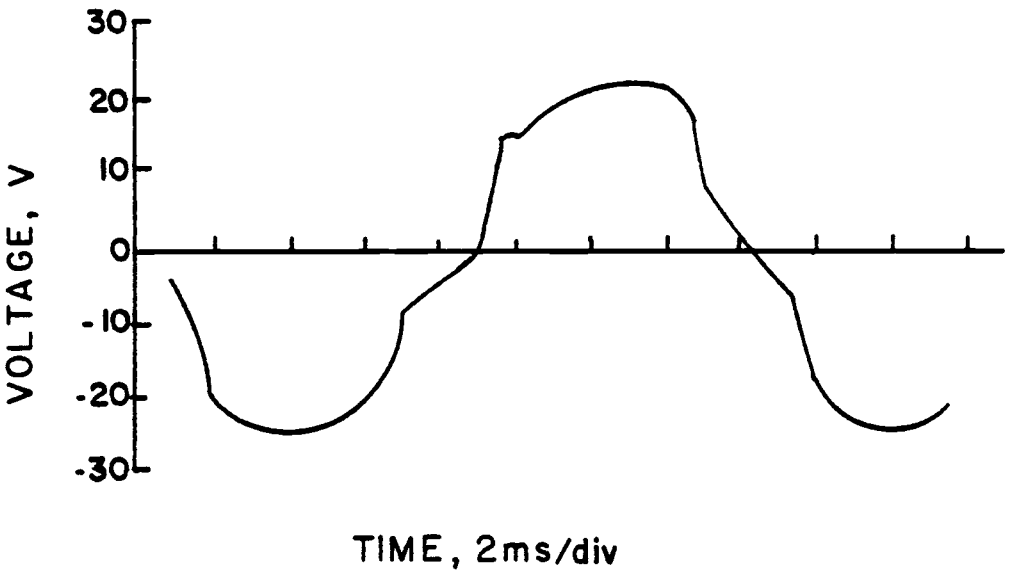

Figure 16. Voltage waveforms across two electrodes.

Electrodes

The plasma arc burns between three 0.040-inch diameter 2% thoriated tungsten electrodes (Tungsten Electrodes, Teledyne Wah Chang, Huntsville, Alabama). The electrodes are planar and 5 mm apart at a 120 degree angle to each other. The electrodes are held in place and connected electrically to electrode holders (Spectrometrics Incorporated, Andover, Massachusetts). The electrode holders (see Figure 17) are continually water cooled, from point D to H, Figure 17, at a water flow rate of 100 ml/min. The electrodes are continually cooled with argon flowing at 0.5 L/min, point I to L, Figure 17, through a removeable metal sheath, point N, Figure 17. A flow rate of 0.5 L/min argon for electrode cooling was the minimum effective flow rate, while flow rates of argon above 2 L/min distorted the plasma shape.

When the plasma arc was operating under the proper conditions, the electrodes were consumed at a rate of less than 1 mm/hr. As the electrodes burn they form a molten globule on the end, which reaches a maximum diameter of approximately 0.080 inches. This globule has no adverse effect on the plasma arc as far as arc wander, and actually the electrodes are consumed at a higher rate than 1 mm/hr without a globule. The only times a globule was not present was if a new electrode was employed or on the rare occasion when the globule was broken off in starting the plasma arc.

Quartz Tubing Assembly

The argon flow and sample aerosol flow to the plasma arc was

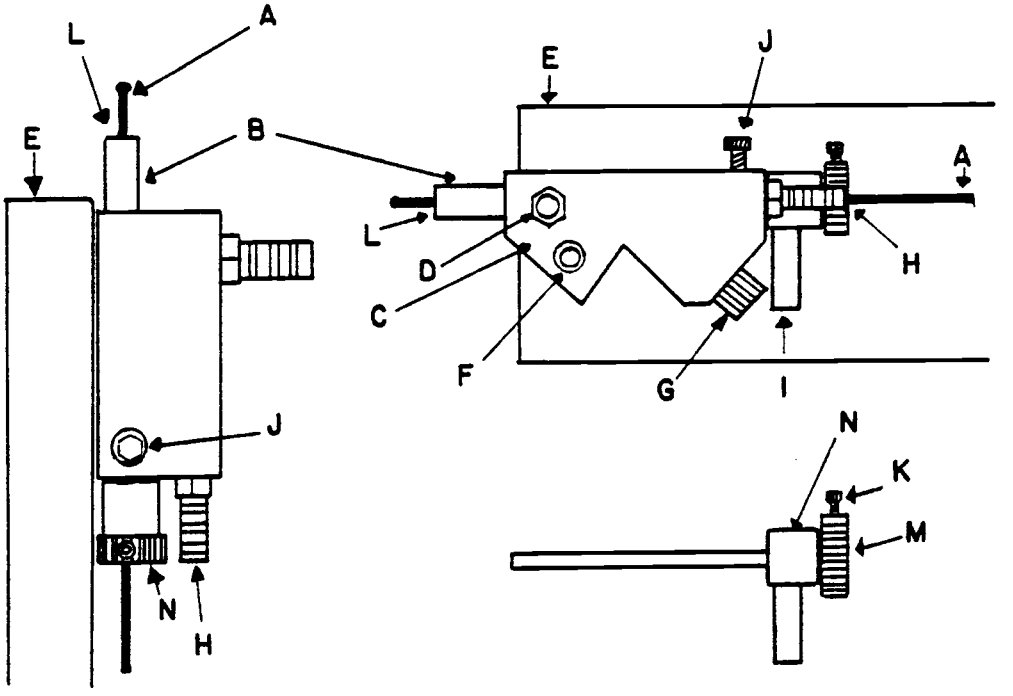

Figure 17. Electrode holders.

A) electrode
B) ceramic cylinder
C) metal body
D) water out
E) Plexiglas
F) bolt connecting electrode holder to plexiglass
G) electrical connection
H) water in
I) argon in
J) bolt to hold N in place
K) bolt to hold electrode in place
L) argon out
M) thumb screw to center electrode
N) removable sheath

accomplished via quartz tubing. Quartz tubing was used rather than glass tubing because of the high temperature of the plasma.

The original quartz tubing assembly consisted of two concentric quartz tubes. The argon to support the plasma flowed through the outer quartz tube and the sample aerosol flowed through the inner quartz tube. However, by adding a third middle concentric quartz tube, a stabler plasma was formed. This three concentric quartz tubing assembly (see Figure 18) is similar to the quartz tubing assembly in the ICP (see Figure 1). The middle quartz tube stablizes the plasma by preventing the flow of argon through the outer tube from pushing the plasma away from the electrodes. Various flow rates of argon were attempted through the middle quartz tube, but no benefit was obtained, as far as plasma stability, at any argon flow rate.

In determining the optimum diameters of the three concentric quartz tubes, several diameters of each quartz tube were tested in various combinations with each other (see Table 3). In the following paragraphs the considerations used for determining the optimum diameters of the three quartz tubes will be discussed.

The inner quartz tube required a small exit orifice so the sample aerosol would have a high velocity to overcome aerodynamic barriers of the plasma. A small exit orifice also produces a small diameter sample aerosol stream, which when introduced into the plasma has less effect on the current flow between the electrodes than a larger diameter sample aerosol stream would. The inner quartz tube required a large entrance diameter to eliminate condensation at the entrance. An inner quartz

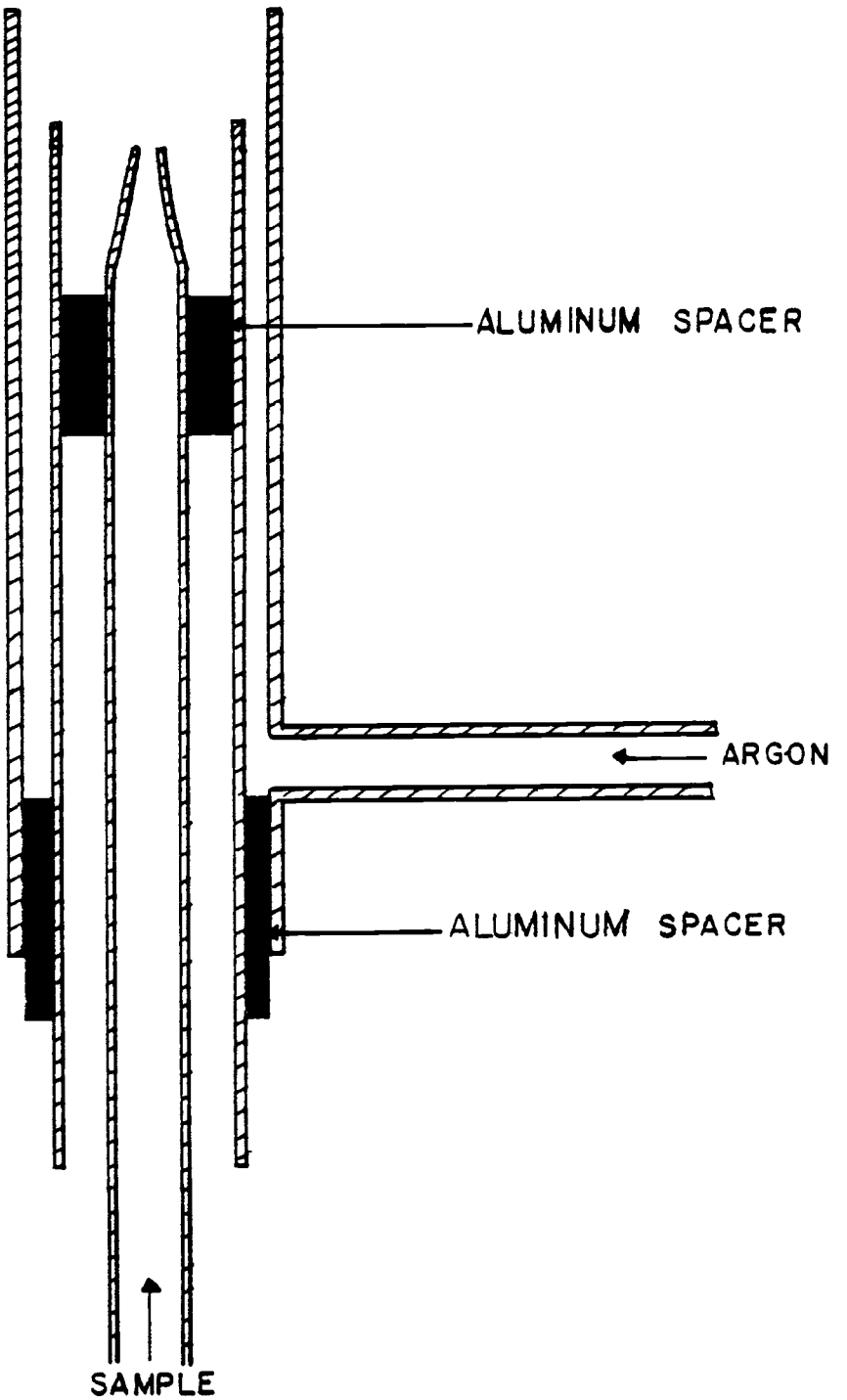

Figure 18. Quartz tubing assembly.

TABLE 3. QUARTZ TUBING ASSEMBLIES SIZES

Configuration		Outer Tube	Middle Tube	Inner Tube
1	o.d. (mm)	26.0	----	4
	i.d. (mm)	24.0	----	3
2	o.d. (mm)	25.0	17.0	4
	i.d. (mm)	21.5	14.5	3
3	o.d. (mm)	21	13.5	8
	i.d. (mm)	19	12.5	6
4	o.d. (mm)	18.5	12.0	8
	i.d. (mm)	15.5	10.0	6
5	o.d. (mm)	16.0	12.0	8
	i.d. (mm)	13.5	10.0	6

tube with a 4-mm o.d. and a 3-mm i.d. was drawn out at the exit end so the exit orifice was 0.3 mm. The entrance diameters were too small and the aerosol tended to condense, so a larger quartz tube was used. The resulting inner quartz tube had diameters of 8-mm o.d. and 7-mm i.d. with the exit end drawn out so the diameter of the exit orifice was 0.3 mm. The inner quartz tube was placed 8 mm below the plasma, so the tip of the tube would not melt. If the distance from the inner quartz tube and the plasma is too large, the sample aerosol spreads out significantly before entering the plasma, resulting in a large diameter sample introduction stream which interferes with the current flow between the electrode causing a noisy plasma.

The choice of the outer quartz tube diameter was influenced by two factors. First, the larger the diameter, the more argon that was required to support the plasma. Next, if the outer diameter of the outer quartz tube was too small, then the corresponding electrode gaps are too small, which resulted in difficult sample introduction for the inner tube that was used. The optimum diameter of the outer quartz tube was 19-mm i.d. and 21-mm o.d.

The outer diameter of the middle quartz tube defined the velocity of the argon flow to the plasma at a given outer quartz argon flow rate. The larger the outer diameter of the middle quartz tube relative to the inner diameter of the outer quartz tube, the more the argon flow is constricted, resulting in higher argon flow velocities to the plasma. A higher argon flow velocity through the outer quartz tube reduced plasma flicker. The limitation encountered was that with a

small distance between the inner diameter of the outer quartz tube and the outer diameter of the middle quartz tube, any misalignment of the two quartz tubes resulted in severe uneven flows of argon to the plasma from one side to another. Misalignment was a problem because the quartz tubes were not fused together and the facilities were not available to fuse the two quartz tubes together. The middle quartz tube diameters used were 12.4-mm o.d. and 13.4-mm i.d. With this quartz tube, a misalignment between the middle and outer quartz tubes resulted in only a small argon flow unevenness. The middle quartz tube was placed approximately 5 mm below the plasma.

The three holes in the outer quartz tube for the three electrodes insertion were 7 mm in diameter. The three holes were 120 degrees apart and 7 mm from the top of the quartz tube, which allowed for viewing the sample emission 10 mm above the electrons. This viewing area is above the high current density portion and high background portion of the plasma yet still relatively close to the excitation portion of the plasma.

Operating the Arc

Prior to igniting the plasma arc, the coolant water, power supply fans, power supply, heating coil, and argon were turned on in that order. A 15-cm, 12-mm i.d. PYREX tube with a 3.5 cm long, 12-mm diameter piece of graphite in the end, was then touched to all three electrodes igniting the plasma. The plasma would ignite with an outer tube argon flow between 3 L/min and 10 L/min. Igniting the plasma with an argon flow through the sample injection tube was difficult, so was avoided.

The outer tube argon flow rate was adjusted to 9 L/min for most emission spectrometry. The sample aerosol was injected into the plasma at a flow rate of about 1 L/min. In Figure 19 is a series of diagrams showing the hole in the center of the plasma produced by sample introduction. Figure 19 is representative of what is seen if the plasma is viewed from above through arc welding mask filters. If the sample injection was not in the center of the plasma, the electrodes were adjusted by moving the posts on which the electrode holders were mounted. Usually alignment prior to igniting the plasma arc was sufficient to obtain proper sample injection into the center of the plasma.

Nebulizer

The modified Babington-type nebulizer was constructed out of plexiglass (see Figure 20). The stainless steel sphere had an orifice of 0.2 mm. This was the smallest orifice that could be drilled in stainless steel with the equipment available. Since a nebulizer based on the Babington principle requires argon flow through this orifice at high pressure for efficient aerosol production, the resulting argon flow into the nebulizer was 2.5 L/min at 60 p.s.i. Since the flow rate was too high for the plasma arc and would either extinguish or produce a very noisy plasma, a split stream system was developed. A split stream system has been used in conjunction with a capacitive microwave plasma (44).

The split stream system was developed so that the sample aerosol

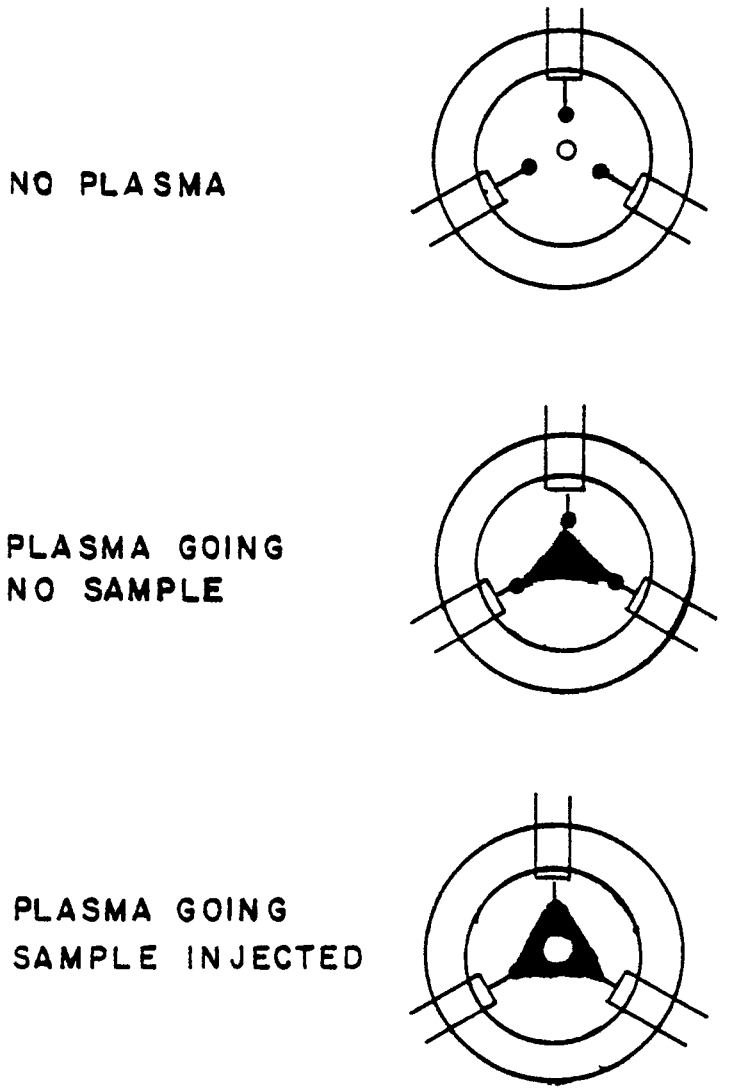

Figure 19. Production of the hole in the plasma.

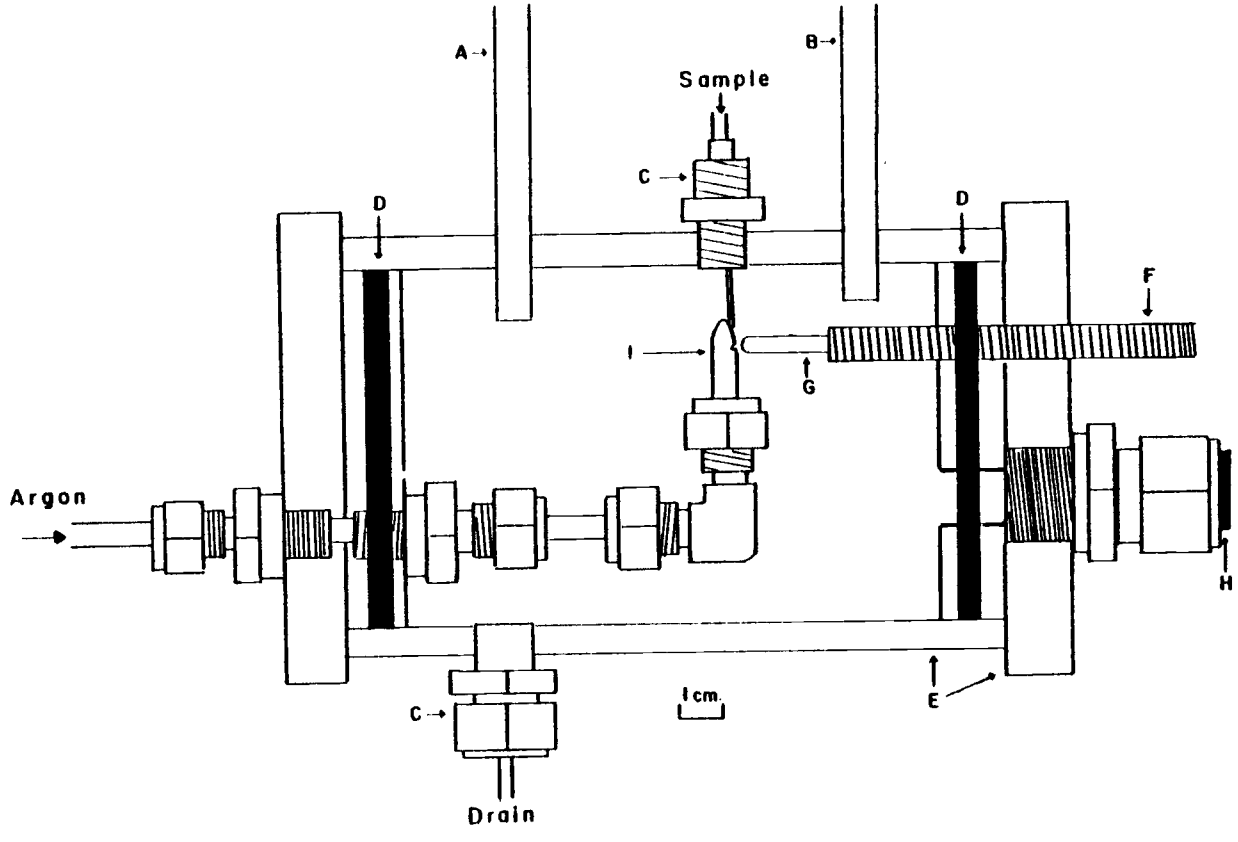

Figure 20. Babington-type nebulizer.

TABLE 4. LIST OF NEBULIZER PARTS FROM FIGURE 20

A.	Quartz Sample Injection Tube
B.	Pyrex Auxillary Sample Tube
C.	Plastic Swagelok (All other Swagelok stainless steel)
D.	O Ring
E.	Plexiglas
F.	Stainless Steel Thread Rod (3/8-32)
G.	Glass Rod
H.	Plug
I.	Stainless Steel Sphere

would travel two similar paths. The exit tip diameter of the sample auxillary tube was varied to obtain the desired argon flow rate to the plasma. This was not difficult because the sample auxillary tube was made out of PYREX. The resulting sample flow was about 1 L/min.

Heating coils made of nichrome wire were wrapped around both the sample injection tube and the sample auxillary tube. The primary function of the heating coils was to prevent sample condensation in the sample tubes. Condensation in the sample tubes results in uneven flows and a noisy plasma. An added advantage of heating the sample aerosol was that less power was required of the plasma to heat the solvent and desolvate the sample. The power supplied through the heating coils was about 25 watts for the sample injection tube and about 20 watts for the sample auxillary tube.

The sample solution delivery to the nebulizer was controlled by a peristaltic pump (Cole-Parmer). The nebulization efficiency was less than 2%. Nebulization efficiency is the ratio of the amount of solution that leaves the nebulizer via the sample tubes to the amount of the sample solution entering the nebulizer. The amount of sample leaving the nebulizer via the sample tubes was estimated by measuring the difference between the amount of sample entering the nebulizer and the amount that remained in the nebulizer.

It has been reported by several workers that one drop of 10% Triton X-100 (alkyl phenoxy polyethoxy ethanol) added to 100 milliliters of sample solution would improve signal stability (45). Triton X-100 is a surfactant which reduces surface tension, and tends to reduce the formation of large drops in the nebulizer chamber. Large drops can

cause turbulence in the flow of fine particles to the plasma. The addition of the Triton X-100 was also reported to aid in overall nebulizer drainage. One drop of 10% Triton X-100 was added to every 100 ml of all sample solutions, with the exception of the sodium solutions, because sodium could have been present in the Triton X-100.

Spectrometric Observation System

A block diagram of the total spectrometric observation system can be seen in Figure 21.

The Aminco Grating Monochromator used was equipped with a 600 grooves/mm grating blazed for 5000 Å first order. The reciprocal linear dispersion is 59 Å/mm first order. The monochromator has a limited scanning range of 15 nm per scan at a scan rate of 10 nm/min. For all studies cited in this thesis a spectral band width of 0.18 nm was used.

A schematic diagram of the current-to-voltage converter can be seen in Figure 22. All Mekee-Pedersen (MP) components were connected in a MP-1001 Console. A 1P28A photomultiplier tube (PMT), in an Aminco (Cat. No. C4-6155) housing, was operated at -725 V. The voltage for the photomultiplier tube was provided by a regulated dc power supply (MP-1002). The anodic current from the photomultiplier tube was converted to voltage by means of a chopper stabilized operational amplifier (MP-1031) with a high impedance resistance selector (MP-1009) set at 10^7 ohms. For most studies, a 1.0 second time constant was used along with a Fluke 8020A Multimeter to measure the voltages. Typical voltages were between 10 mV and 1 V. For the background emission scans,

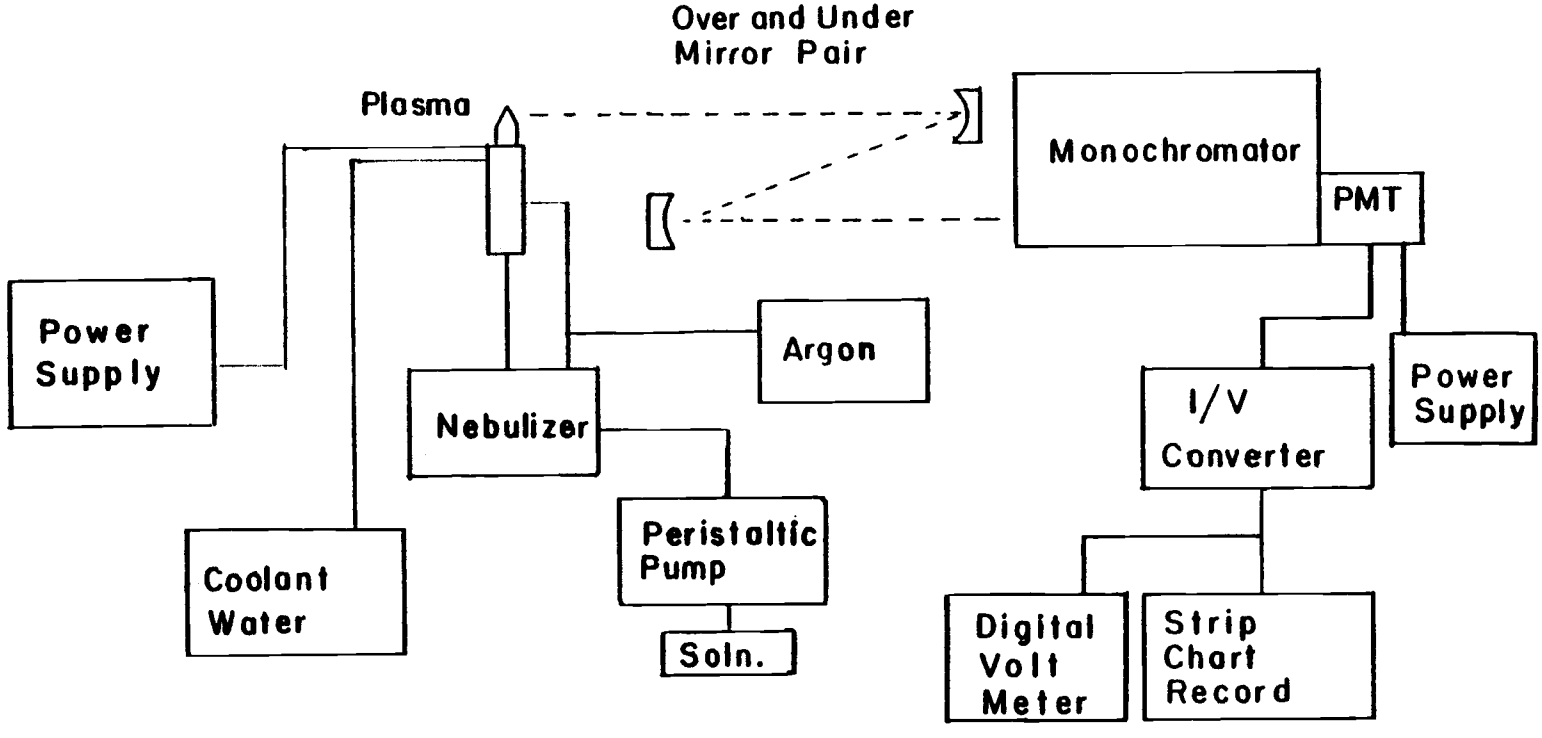

Figure 21. Block diagram of total spectrometric observation system.

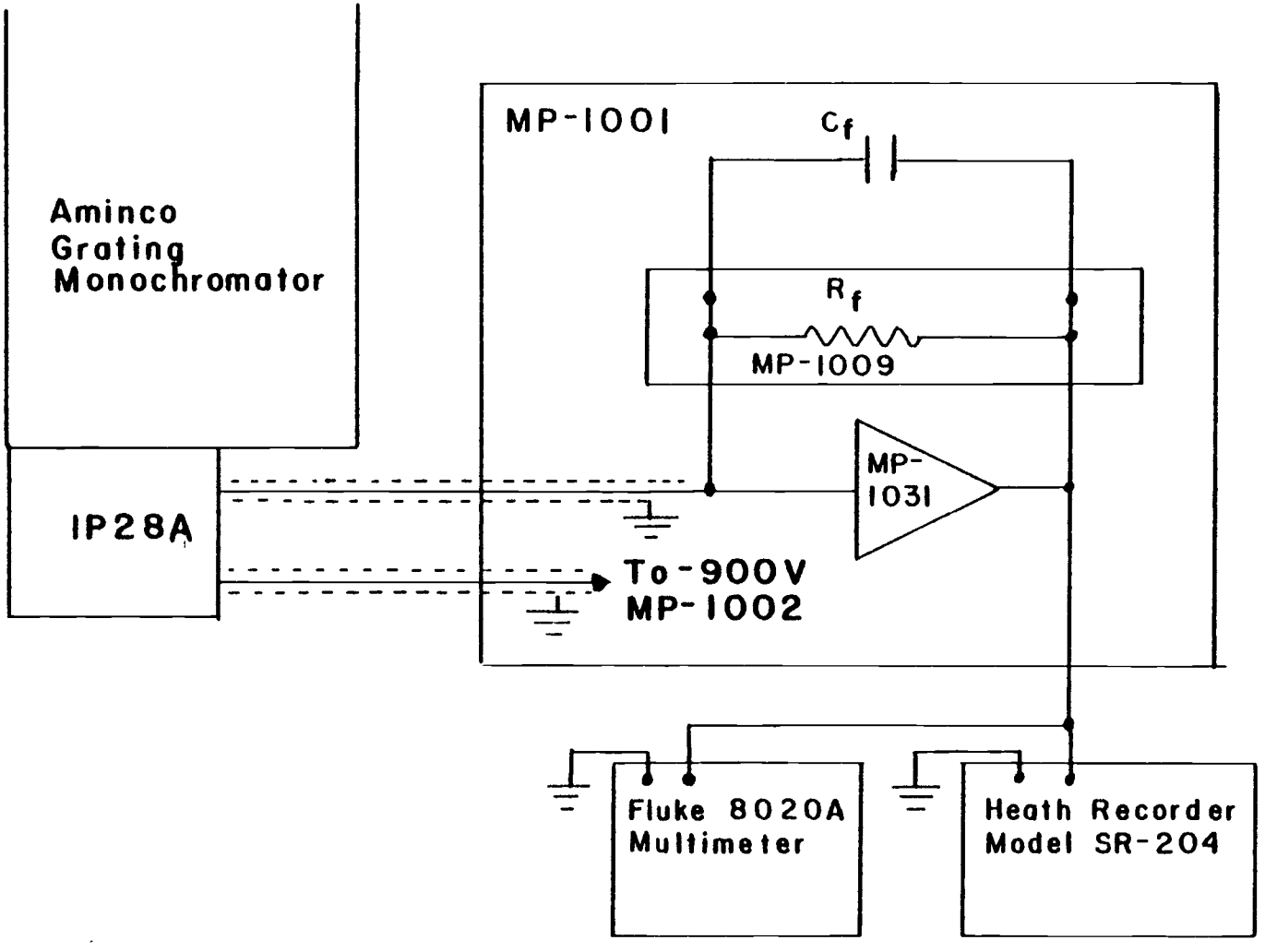

Figure 22. Schematic of current to voltage conversion.

and a few other studies, a 0.1 second time constant was used along with a Heath Model SR-204 Strip Chart Recorder.

Emission measurements were made from the plasma via two 350-mm focal mirror aluminized with a MgF_2 coating for high reflectance in the UV wavelength region. The mirrors were mounted in the over-and-under configuration to reduce astigmatism produced by the side-by-side mirror configuration in the monochromator (46). The mirror mounts enabled independent control of the pitch and yaw, which provided calibrated adjustments of the emission viewing region both vertically and horizontally.

Reagents

Standard dilution from the stock solutions shown in Table 5 were used for all studies. These solutions were prepared according to procedures described by Dean and Raines (47) with the exception of aluminum and strontium. All solutions were prepared with millipore water, reagent grade chemicals, and stored in polyethylene containers.

TABLE 5. REAGENTS

Desired Solution	Procedure
1000 mg/L copper	1.000 g. of Cu foil was placed in 10 mL of concentrated HNO_3 and 5 mL of water to which concentrated HCl was added dropwise until the Cu dissolved. The solution was boiled to expel oxides of nitrogen and chlorine, then diluted to 1 L.
100 mg/L sodium	2.5421 g. of NaCl was dissolved in water and diluted to 1 L.
1000 mg/L aluminum	12.3495 g. of $Al_2(SO_4)_3 \cdot 18\ H_2O$ was dissolved in water and diluted to 1 L.
1000 mg/L barium	1.7787 g. of $BaCl_2 \cdot 2\ H_2O$ was dissolved in water and diluted to 1 L.
1000 mg/L nickel	1.000 g. of Ni was dissolved in 10 mL hot concentrated HNO_3. The solution was cooled and diluted to 1 L.
1000 mg/L manganese	1.000 g. of Mn was dissolved in 10 mL concentrated HCl plus 1 mL concentrated HNO_3, then diluted to 1 L.
1000 mg/L strontium	2.4155 g. of $Sr(NO_3)_2$ was dissolved in water and diluted to 1 L.

RESULTS AND DISCUSSION

Nebulizer Characteristics

To determine the optimum solution flow rate to the nebulizer, a 100 mg/L barium solution as well as a blank solution were pumped, via a peristaltic pump, to the nebulizer at various flow rates and the resulting emission signal at 455.4 nm was measured. The voltage measurements were made with a meter using a one second RC time constant. A plot of the net relative emission for the 100 mg/L barium solution versus the sample flow rate is shown in Figure 23. In Figure 23 it can be seen that the relative emission signal increases with sample solution flow rate, but so does the noise, as indicated by the bars at each point. A plot of S/N versus sample flow rate using the same data is shown in Figure 24. The signal (S) was calculated as the mean value of the 100 mg/L barium solution signal minus the mean value of the blank solution signal. The noise (N) was calculated as the standard deviation of the 100 mg/L barium solution signal minus the standard deviation of the blank signal. As can be seen, the noise increases dramatically at high solution flow rates. At higher flow rates the sample solution probably no longer produces a thin film over the Babington sphere, rather, a thick film is probably produced which results in large droplet formation during the nebulization process. The optimum flow rate was 18 mL/min which was used for all the experiments in this thesis.

The optimum sample solution flow rate of 18 mL/min is higher than the 5 mL/min sample solution flow rate utilized in a Babington-type

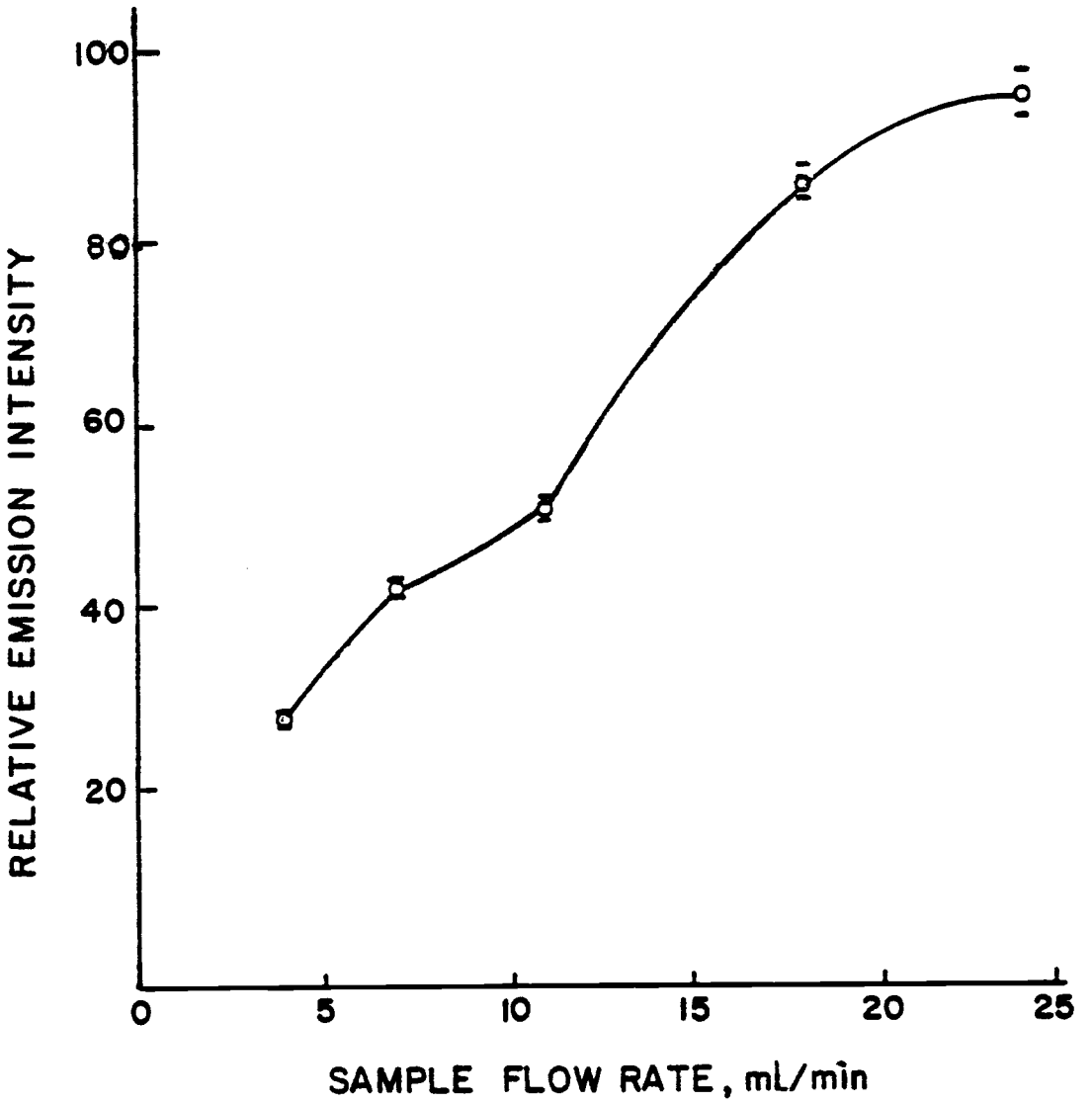

Figure 23. Plot of relative emission intensity versus sample solution flow rate to the nebulizer.

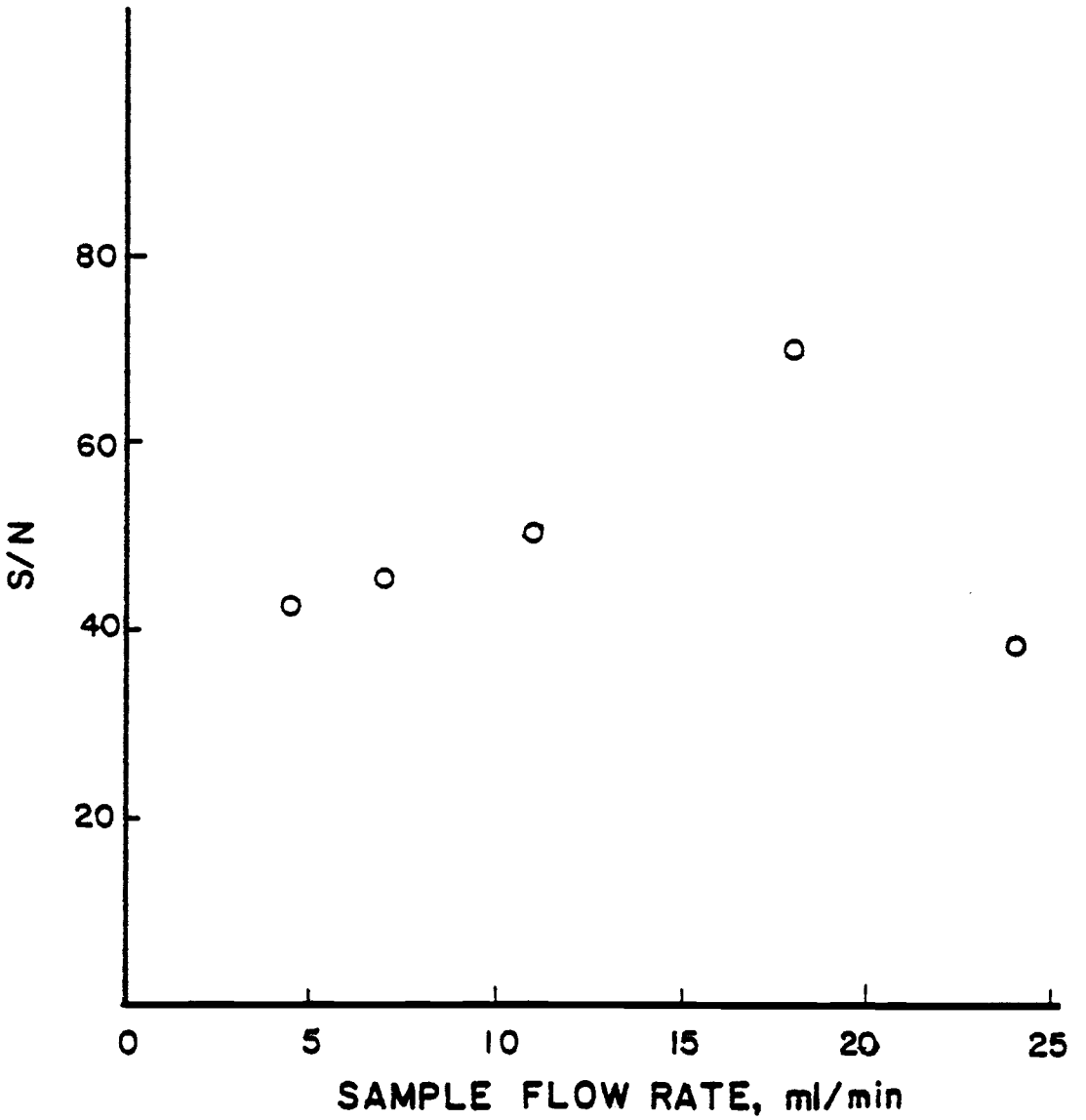

Figure 24. Plot of S/N versus sample solution flow rate to nebulizer.

nebulizer used in conjunction with the ICP (39). A possible reason for the higher sample solution flow rate is that the diameter of the exit orifice in the Babington sphere in my nebulizer is larger, resulting in an argon flow rate of 2.2 L/min through the exit orifice compared to 1.0 L/min in the Babington-type nebulizer used in conjunction with the ICP.

To determine the response time of my nebulizer, a sample solution of 500 mg/L barium was nebulized into the plasma, and the emission intensity was measured at 455.4 nm. The 500 mg/L barium solution was then replaced by a blank solution and the emission signal decay was measured every 5 sec. After a stable blank signal was obtained, the blank solution was replaced with the 500 mg/L barium solution and the emission signal increase was measured every 5 sec. A plot of relative emission intensity versus time can be seen in Figure 25. The response time, or the time required to reach 63% of the new signal, is 10 sec. The response time is limited by the length of the 1 mm i.d. Tygon tubing from the peristaltic pump to the nebulizer and the size of nebulizer chamber.

Heating Coil

To measure the effect the heating coil had on the intensity of an emission signal, a 100 mg/L barium solution was nebulized into the plasma, with the heating coil off. The emission signal was measured at 455.4 nm and recorded on a strip chart recorder with a 0.1-second time constant. After a stable signal was obtained the heating coil was turned on. The emission signal increased and when the emission signal

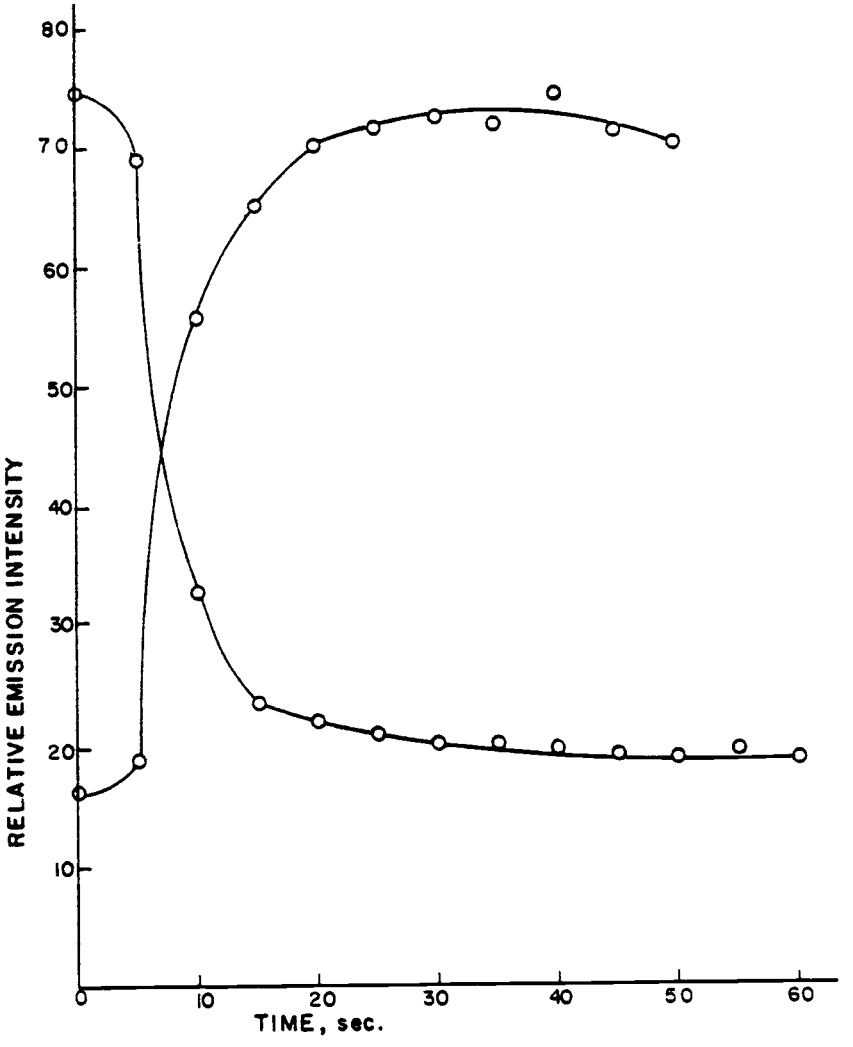

Figure 25. Response of nebulizer.

reached a new stable level the heating coil was turned off. The emission signal decayed down to approximately the original level before the heating coil had been turned on. The net signal increase due to having the heating coil on was about 30%.

Background Emission

A spectrum of the background emission was obtained over the wavelength region 600-250 nm (see Figure 26). All of the 70 nm scans shown in Figure 26 are not at the same scale sensitivity due to the fact that the optical efficiency of the spectrometer varied over the 600-250 nm wavelength region. The background spectrum was obtained with no blank solutions introduced into plasma.

The peaks in the background emission spectrum correspond to tungsten emission lines. The tungsten emission results from the use of 98% tungsten electrodes. The other 2% of the electrodes is thorium. No peaks corresponding to thorium emission were seen above the background in the background emission spectrum. No peaks corresponding to argon emission above the background were seen in the background emission spectrum either.

The background emission signal increased as wavelength decreased, 600-450 nm, in the background emission spectrum (see Figure 26). This was due in part to the fact that the grating of the monochromator was blazed at 600 nm, and as you move away from the wavelength at which the grating was blazed, the stray light increases (48). Although the stray light was increasing below 450 nm, the background emission

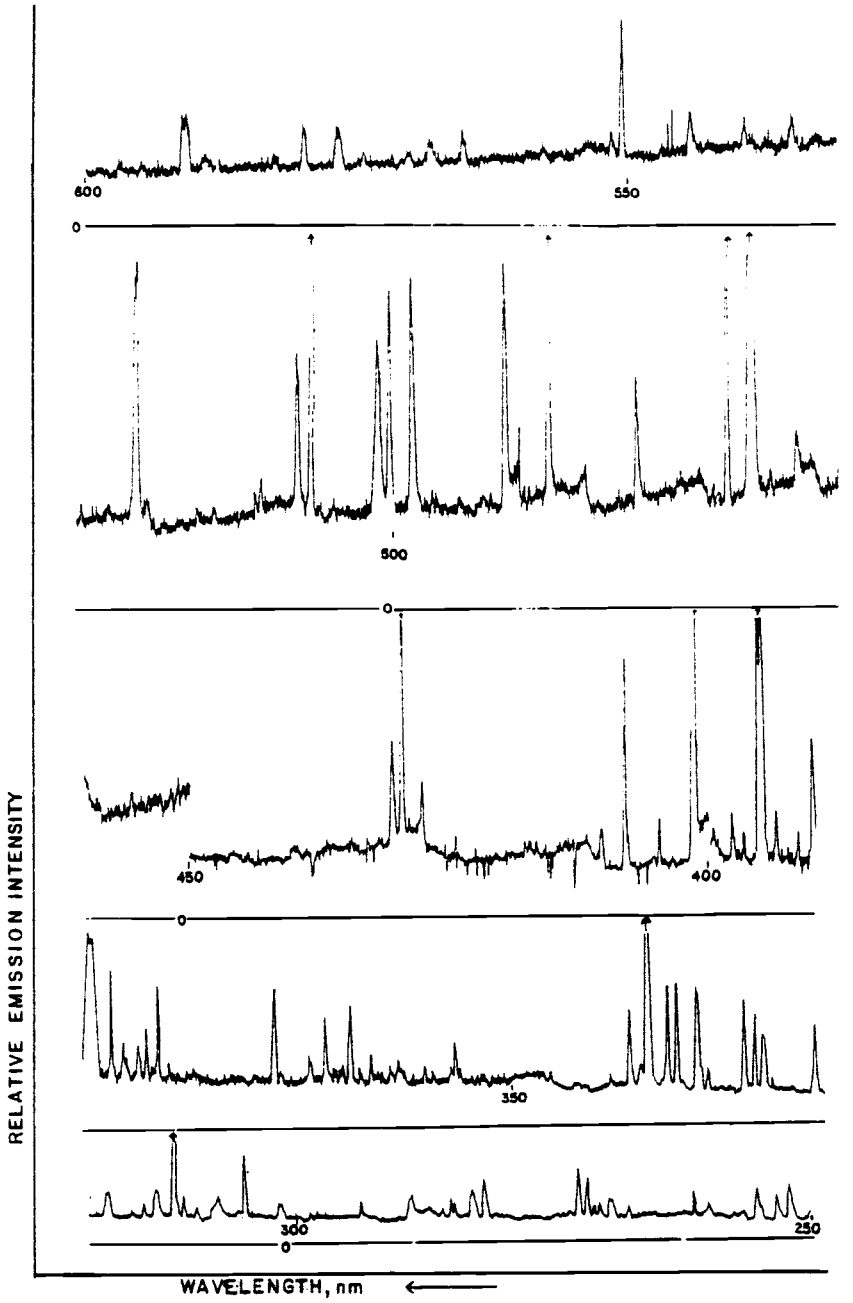

Figure 26. Background Emission Spectra.

intensity was decreasing, Figure 26. This was because the optical efficiency was decreasing gradually, and although the background was decreasing so was the signal to background ratio.

Since there are so many tungsten lines, a background emission spectrum was very useful in selecting the wavelengths free from background interferences for analytical emission analysis. An alternate method of determining possible interfering background lines would be to simply look up the relative intensities of tungsten lines for the wavelength region of interest in a table of spectra lines. The relative intensities of the tungsten lines in the background emission scans (Figure 26) correlated reasonably well with the table of spectral lines.

Noise in Background Signal

The noise in the background signal usually limits the detection limit in analytical emission spectrometry. A calculation of the background noise components of the emission signal was obtained for a blank solution as described by Ingle (49).

The background signal intensity was determined by making repetitive voltage readings of a blank solution at 324.7 nm. The time constant was 1.0 sec, so readings were taken every 5 sec.

The standard deviation of the blank signal σ_{b+d} is the noise in the blank signal. The value obtained for σ_{b+d} was 1.3×10^{-4} V.

Theoretically

$$\sigma_{b+d} = [\sigma_{dt}^2 + (\sigma_b)_{q+s}^2 + (\sigma_b)_f^2]^{1/2} \qquad (5)$$

where σ_{dt}^2 = dark current noise

$(\sigma_b)_{q+s}$ = background shot noise

$(\sigma_b)_f$ = background source flicker noise.

The background shot noise can be calculated from:

$$(\sigma_b)^2_{q+s} = mR_fKE_b \qquad (6)$$

where m = PMT gain = 3.5×10^5

R_f = feedback resistor = $10^7\ \Omega$

E_b = blank signal = 9.0×10^{-3}V

$K = 2e\Delta f\ (1+\alpha)$

where $e = 1.6 \times 10^{-19}$C

$\Delta f = 1/4\tau$, $\tau = R_fC_f = 1.0$ sec

estimate $\alpha = 0.3$

$K = 2\ (1.6 \times 10^{-19}\text{C})\ 1/4\ \text{sec}\ (1+0.3)$

$K = 1.04 \times 10^{-19}$A

Substituting the values in Equation (6)

$$(\sigma_b)^2_{q+s} = 3.5 \times 10^5 (10^7\Omega)\ 1.1 \times 10^{-19}\text{A}\ (9.0 \times 10^{-3}\text{V})$$

$$(\sigma_b)^2_{q+s} = 7.1 \times 10^{-9}\text{V}^2$$

Experimentally the noise in the dark current voltage was obtained by making repetitive measurements of the dark current voltage with light blocked to the PMT, and calculating the standard deviation. The value obtained for the dark current noise was 3.2×10^{-5}V.

Rearranging Equation (6) and substituting in the appropriate values, the flicker noise can be calculated

$$(\sigma_b)_f = [\sigma_{(b+d)}^2 - \sigma_{dt}^2 - (\sigma_b)_{q+s}^2]^{1/2} \quad (7)$$

$$(\sigma_b)_f = [(1.3 \times 10^{-4}V)^2 - (3.2 \times 10^{-5}V)^2 - 7.1 \times 10^{-9}V^2]$$

$$(\sigma_b)_f = 1.2 \times 10^{-4}V.$$

It is apparent that the major source of noise in the background signal is background flicker, which is usually the case when there is a high background signal like that seen with this three-phase plasma arc.

Plasma Regions

To determine the various regions of the plasma a 100 mg/L sodium solution was nebulized in the plasma. Visually viewing the plasma through a UV rejection filter several distinct regions of the plasma could be seen, and are shown in Figure 27. A very intense orange color was seen in the central sample region which was due to the sodium emission. The plume, Figure 27, was also orange, but not as intense as the center. The plasma region, Figure 27, appeared greenish through the UV rejection, visible attenuation filter.

Emission Profile of the Plasma

The profile of the net emission intensity from a 500 mg/L nickel solution, measured at 352.4 nm, versus the horizontal distance from the center of the plasma and the vertical distance above the electrodes is plotted in Figure 28. The area viewed by the spectrometer was calibrated by backlighting the monochromator and calibrating the micrometers on the mirror mounts, which independently controlled the vertical

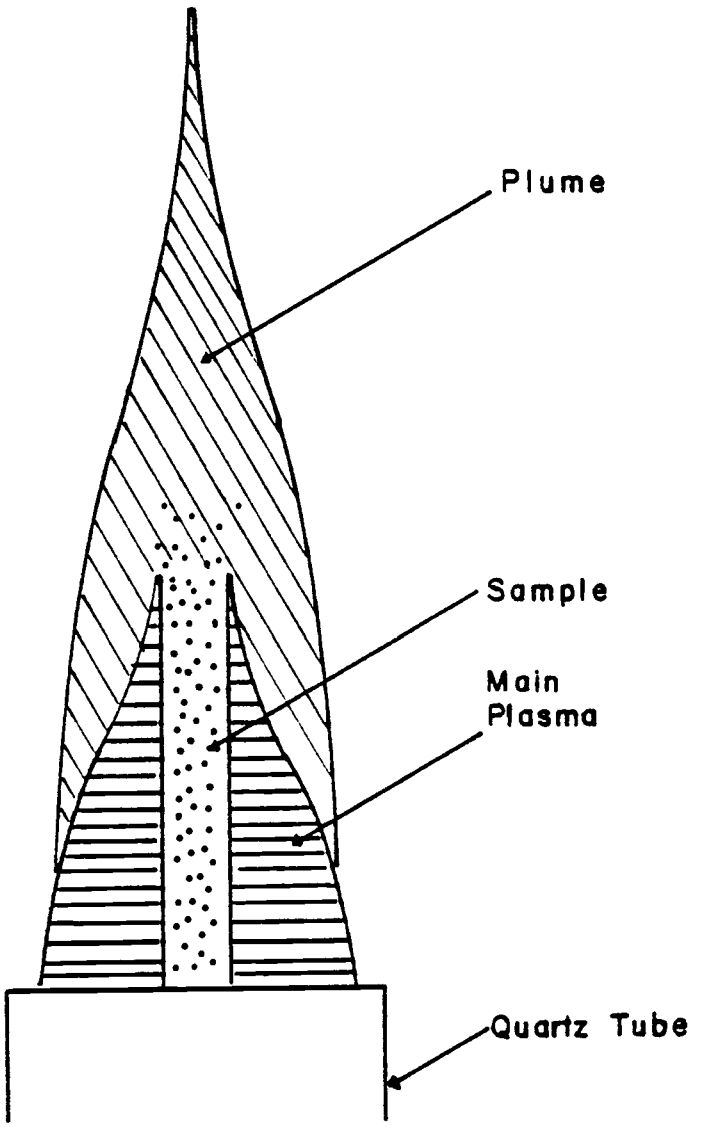

Figure 27. Plasma regions.

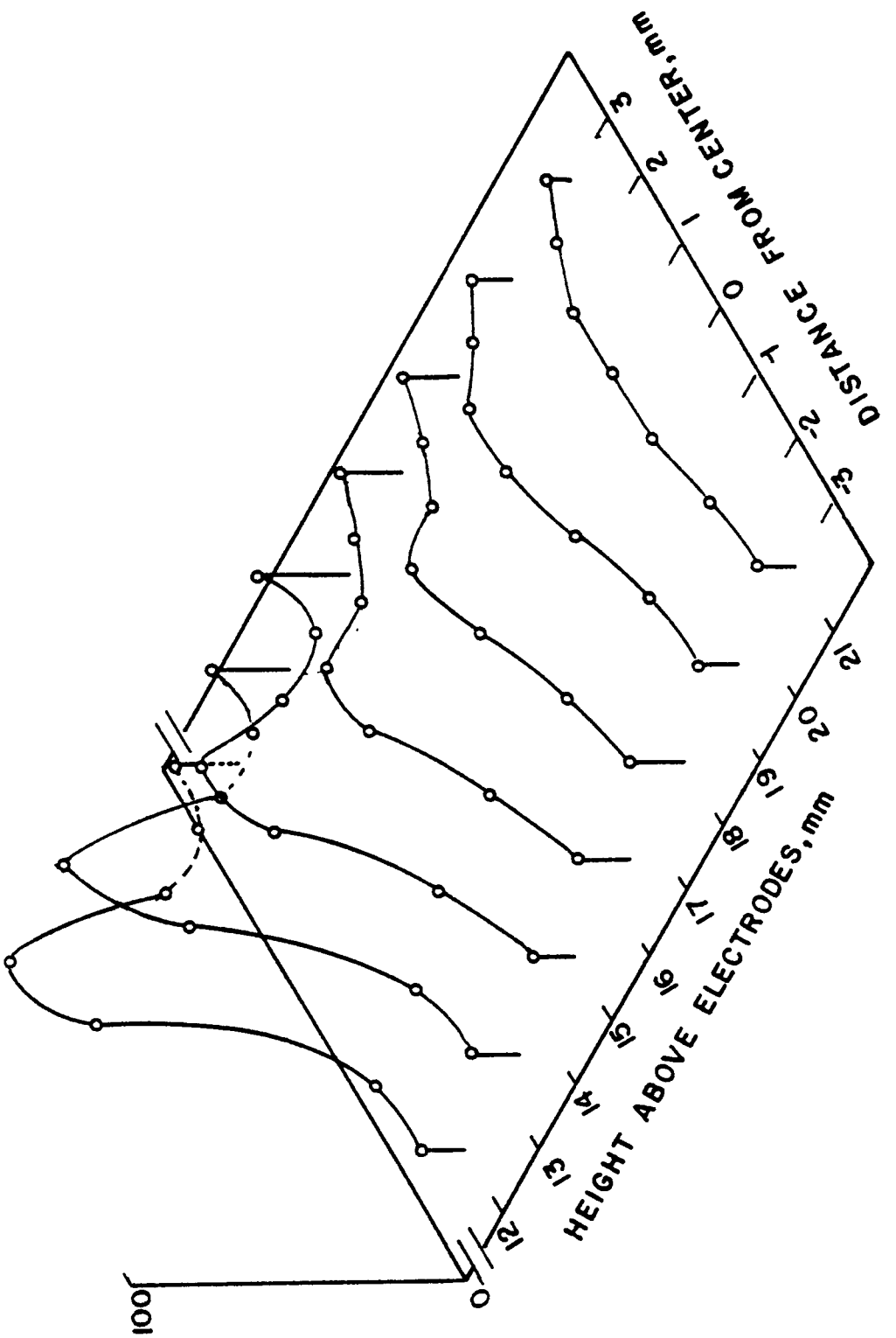

Figure 28. Profile of nickel emission in plasma.

and horizontal position of the viewing region, as previously described in the instrumentation section. The outer quartz tube limited viewing any lower than 12 mm above the electrodes.

As can be seen from the plot of relative emission signal in Figure 28, the net emission signal is largest in the center of the plasma closest to the electrodes. The emission signal should be strongest in the center since the sample is introduced in the center of the plasma. The emission signal is largest closer to the electrodes where the plasma is hottest.

A profile of the emission intensity from a blank solution was also plotted (see Figure 29). The relative emission intensity scales for Figure 28 and Figure 29 are different. The background emission profile has a similar shape compared to the 500 mg/L nickel emission profile, but does not decrease as rapidly with height.

Calibration Curves

Calibration curves were obtained for copper, sodium, and aluminum at 324.7 nm, 588.9 nm, and 309.2 nm respectively. These three elements were chosen because they represent three distinct types of elements. Copper is a transistion metal and usually works well for analytical emission spectrometry. Sodium is an alkali metal with a low ionization potential. In the high temperature plasmas sodium has a tendency to ionize, whereas in the lower temperature flames sodium doesn't ionize as much. Aluminum forms a refractory oxide which requires higher temperatures to atomize.

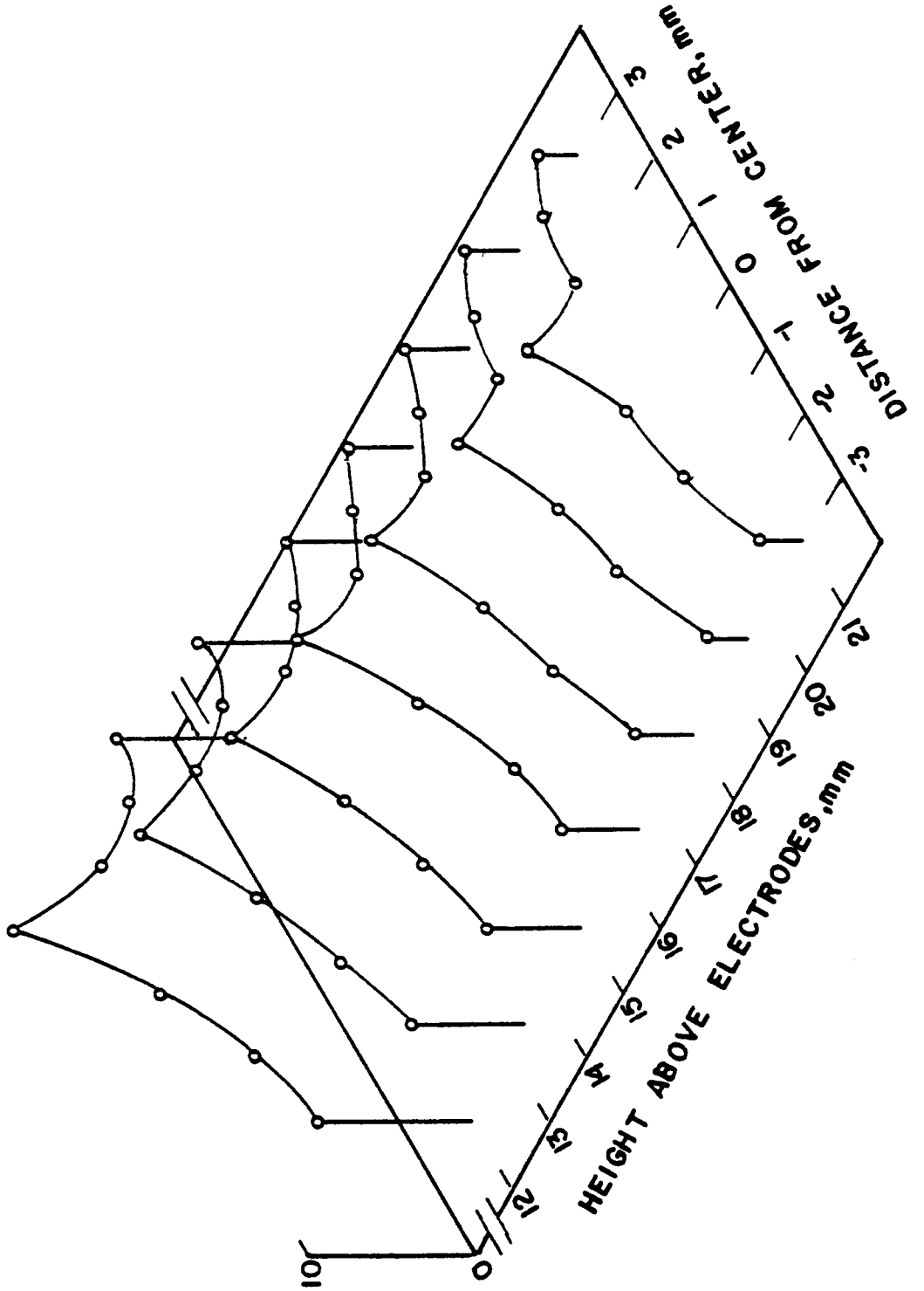

Figure 29. Profile of background emission in plasma.

The argon and sample flow conditions for obtaining the copper and sodium calibration curves were essentially the same; a 1 L/min sample aerosol flow rate to the plasma and an outer tube argon flow rate of 9 L/min. Under these operating conditions aluminum yielded a very low intensity emission signal even at high concentration levels. By lowering the sample aerosol flow rate to the plasma and lowering the outer tube argon flow rate, the aluminum emission increased by over an order of magnitude. The sample aerosol flow rate was approximately 0.5 L/min and the argon outer tube flow rate was 6 L/min.

The lower sample aerosol flow probably enabled a longer residence time for the sample in the plasma and the lower argon flow rate through the outer tube resulted in a higher plasma temperature, which would increase the atomization efficiency of the aluminum. The lower outer tube argon flow resulted in a less aerodynamically stable plasma, which increased the noise.

The emission signal from sodium and copper were also evaluated at these lower argon and sample aerosol flow rates. Copper gave a slightly lower emission signal at these lower flow rates than was obtained at the higher flow rates. A possible explanation for this is the fact that less sample per unit time is entering the plasma so the total copper population was lower.

The sodium emission signal at these lower flow rates was much less than at the higher flow rates. This may have been due to increased ionization of the sodium, and the wavelength monitored, 589.0 nm is not an ion line. An attempt was made to view the sodium ion line

at 288.1 nm, but due to the fact it is three orders of magnitude less intense than the unionized sodium line 589.0 nm in the ICP (50), and the fact that there is an intense tungsten line at 287.9 nm , the sodium ion line at 288.1 nm could not be seen in the three-phase plasma arc above the background emission.

The slopes of the three calibration curves were calculated using linear regression from an HP 35E calculator. The error in the slope was calculated using a standard formula for calculating the error in the slope (51).

The slope of the copper calibration curve, without the 1000 mg/L data point, is 0.98 ± 0.08 for the log-log plot of concentration versus relative emission intensity, Figure 30. The slope of the sodium calibration curve, without the 1000 mg/L data point, Figure 31 is 1.07 ± 0.04 for this log-log plot of concentration versus relative emission intensity. The slope of the aluminum calibration curve using all the data points is 0.89 ± 0.06 for the log-log plot of the concentration versus relative emission intensity, Figure 32.

A slope of 1.00 indicates that the relationship between the emission signal and concentration is linear and passes through the origin. Within the error of the slope, copper has a slope of one and sodium has a slope close to one. Aluminum has a slope slightly less than one which could result from self absorption or from the fact that the standards were made from salts and at high salt concentration the larger salt particles size can result in inefficient atomization. At 1000 mg/L the sodium and copper calibration curves

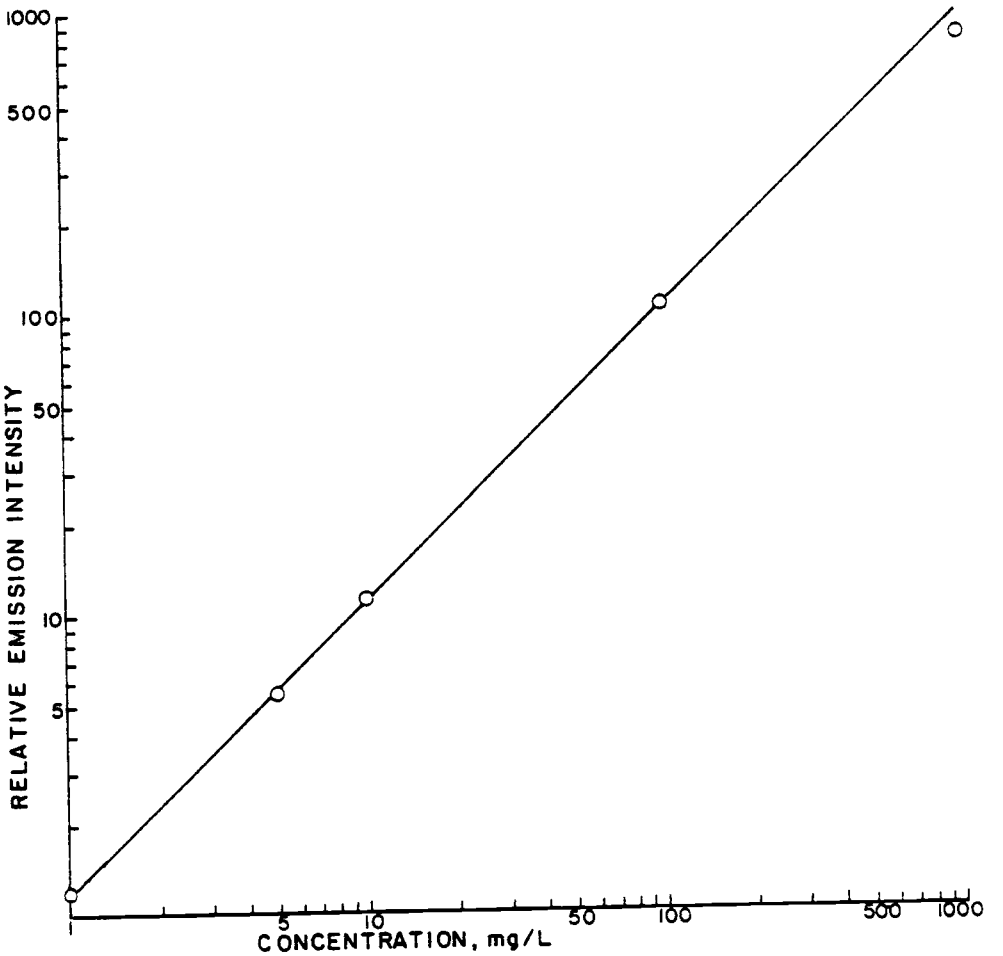

Figure 30. Copper calibration curve.

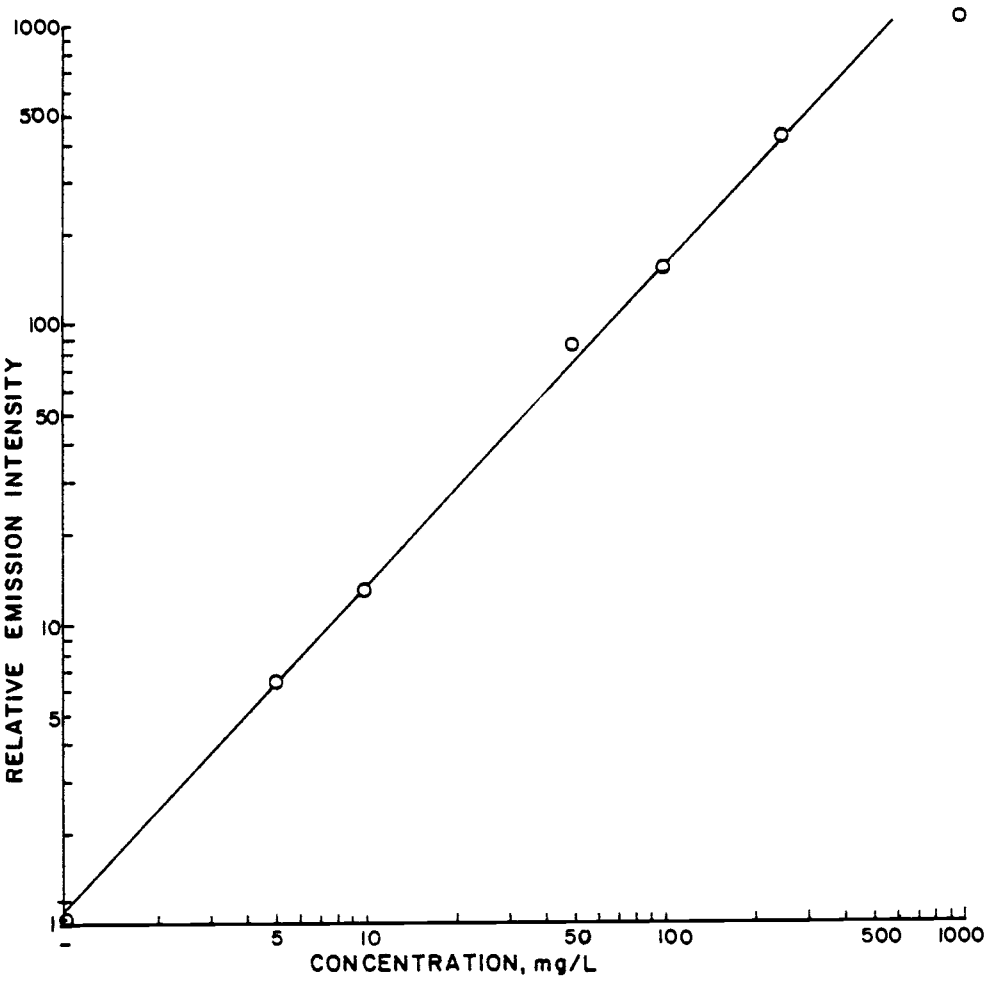

Figure 31. Sodium calibration curve.

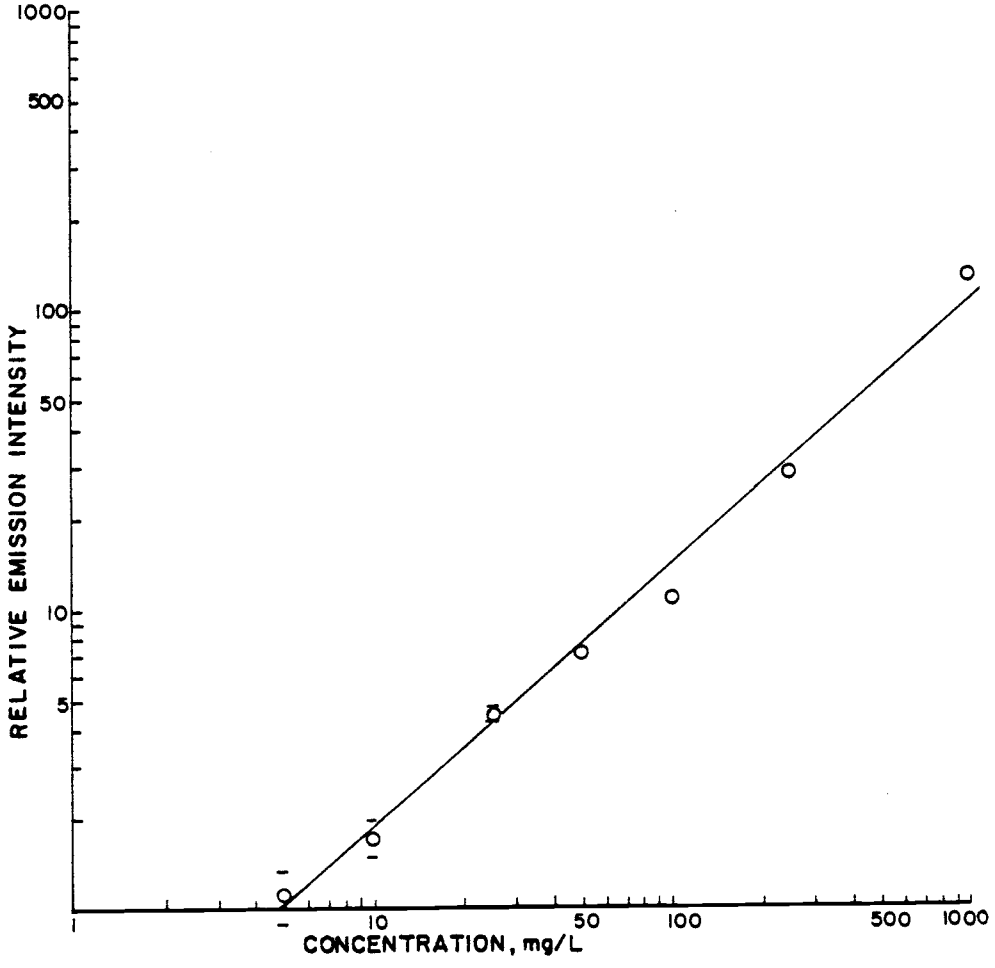

Figure 32. Aluminum calibration curve.

showed negative deviations due to either self absorption or the high salt concentration.

The linear dynamic concentration ranges for the copper, sodium, and aluminum are approximately three orders of magnitude, if the assumption is made that the calibration curves are linear down to the detection limits, which will be presented in the next section. The linear dynamic concentration range for the three-phase plasma compares favorably with the DCP linear dynamic concentration ranges of two to three orders of magnitude (52), considering that the actual concentrations used for the three-phase plasma arc linear dynamic concentration range are one to two orders of magnitudes larger than the concentrations used for the DCP linear dynamic concentration range. The linear dynamic concentration range for the ICP is 10^5-10^6 (21), which is far superior to either the three-phase plasma arc or the DCP.

Detection Limits

Detection limits for several elements were determined. The definition of detection limits in a chemical flame as described by Vickers and Winefordner was used.

> The detection limit is the concentration of the element in solution which when aspirated into a plasma gives an emission signal equal to twice the standard deviation in the background emission (53).

Detection limits for seven elements are given in Table 6, as well as the wavelength used and detection limits reported for the ICP and DCP.

TABLE 6. DETECTION LIMITS (μg/L)

element	λ(nm)	TPP	DCP	Lit.	ICP	Lit.
copper	324.7	100	5	(52)	1	(39)
sodium	589.0	300	-		0.2	(54)
nickel	341.4	-	10	(52)	-	
	352.4	200	-		6	(13)
manganese	257.6	-	-		0.04	(39)
	403.1	300	20	(52)	-	
strontium	407.8	400	-		0.3	(39)
aluminum	309.2	2000	-		-	
	396.1	-	5	(52)	2	(13)
barium	455.4	500	-		0.4	(39)

The ICP detection limits chosen for comparison with the three-phase plasma arc detection limits were the detection limits obtained with an ICP using a Babington-type nebulizer (39). For those elements for which a detection limit was not determined by an ICP with a Babington-type nebulizer, the best available detection limits for an ICP using other pneumatic nebulizers (13, 52) were used to compare to the detection limit obtained with a three-phase plasma.

The detection limits for the three-phase plasma arc are between a factor of 15 to 400 higher than the detection limits reported for the DCP, and a factor of 33-1200 higher than the detection limits reported for the ICP.

There are several possible ways in which the detection limits in the three-phase plasma arc could be improved. First, more power supplied to the plasma should help lower the detection limits by exciting more atoms. Second, if a monochromator with a grating blazed at a lower wavelength were employed, it would reduce the stray light in the background signal. The last possible way to improve detection limits would be to make the three-phase plasma arc more aerodynamically stable, reducing the flicker noise in the background.

CONCLUSIONS

The new three-phase argon plasma arc described in this thesis is the only argon plasma, besides the ICP, to a have an area of lower electron density in the center of the plasma for effective sample aerosol introduction into the plasma. The effectiveness of the sample aerosol introduction into the center of the plasma was determined by viewing the emission profile across the plasma visually and spectrometrically.

A circuit was developed that utilized bipolar junction transistors to control the current flow through the plasma. The circuit worked briefly but then the transistors failed due to the large power dissipated across the transistors. A simple circuit was then designed to control the current to the plasma. This simple circuit had less current control capabilities than the transistor circuit did. However, no information was obtained as to what effect any possible current changes had in the plasma or visa versa.

A three concentric quartz tubing assembly is the best configuration found in this study for supplying argon and sample aerosol to the plasma. A three concentric quartz tubing assembly with the tubes fused into position is suggested for future work with the three-phase plasma arc because it eliminates tubing misalignment, and if constructed properly could enhance the plasma aerodynamic stability at lower argon flow rates.

The Babington-type nebulizer constructed for use with the three-phase plasma worked satisfactorily. However, if a smaller exit orifice

in the Babington sphere could be made, it would eliminate the need for a sample aerosol split stream and would conceivably use less sample solution and less argon.

The 25 W heating coil used for sample aerosol vaporization enhanced the emission signal by 30%, as well as eliminated sample condensation in the sample aerosol tubes.

The three-phase argon plasma arc exhibited many of the same properties of an ideal excitation source as do the ICP and DCP. Some of the properties of an ideal source in which this three-phase plasma arc was not as good as the ICP or DCP were dynamic range, detection limit, and freedom from spectral interferences. The linear dynamic concentration range of the three-phase plasma arc was comparable to the DCP, but two to three orders smaller than linear dynamic concentration range of the ICP. The detection limits for seven elements in the three-phase plasma arc were a factor of between 15-400 times higher than the detection limits reported for the DCP, and a factor of 33-1200 times higher than the detection limits reported for the ICP. The tungsten background emission from the electrodes is an interferent present in the three-phase plasma arc not present in the ICP or DCP. There are so many tungsten lines that they limit to some degree the total number of emission lines available for analysis, as well as contribute to the background continuum. The use of carbon electrodes would reduce spectral interferences considerably.

An advantage the three-phase plasma arc has over the DCP and ICP is initial cost, because of the simplicity of the power supply. The

three-phase plasma arc also uses about half the power that the ICP or DCP does, and uses 30% less argon than the ICP.

The key to future success for the three-phase plasma arc for analytical emission spectrometry is better aerodynamic stability at lower argon flow rates and better detection limit. Detection limits might be improved by better aerodynamic stability and higher power dissipation in the plasma.

BIBLIOBRAPHY

1. V. A. Fassel, Quantitative Elemental Analysis by Plasma Emission Spectroscopy, Science 202, 183-191 (1978).

2. S. Greenfield, the Inductively Coupled Plasma Torch-A Source for all Reasons, The Spex Speaker 12, 1 (1977).

3. T. B. Reed, Induction-Coupled Plasma Torch, J. Appl. Phys. 32, 821 (1961).

4. T. B. Reed, Growth of Refractory Crystals Using the Induction-Plasma Torch, J. Appl. Phys. 32, 2534 (1961).

5. S. Greenfield, I. L. W. Jones, and C. T. Berry, High-Pressure Plasmas as Spectroscopic Emission Sources, Analyst 89, 713 (1964).

6. R. H. Wendt and V. A. Fassel, Induction-Coupled Plasma Spectrometric Excitation Source, Anal. Chem. 37, 920 (1965).

7. R. H. Wendt and V. A. Fassel, Atomic Absorption Spectroscopy with Induction-Coupled Plasma, Anal. Chem. 38, 337 (1966).

8. S. Greenfield, P. B. Smith, A. E. Breeze, and N. M. D. Chilton, Atomic Absorption with an Electrodeless High-Frequency Plasma Torch, Anal. Chim. Acta 41, 385 (1968).

9. W. B. Barnett, V. A. Fassel, and R. N. Kniseley, Theoretical Principles of Internal Standardization in Analytical Emission Spectroscopy, Spectrochim. Acta, Part B, 23, 643 (1968).

10. M. E. Briske, V. M. Borigor, and Yu S. Sukah, Ind. Lab. 33, 301 (1967).

11. C. Bordonale, M. A. Biancifiori, A. Donata, and B. Morello, Metall. Ital. 61, 360 (1969).

12. C. Veillon and M. Margoshes, An Evaluation of the Induction-Coupled, Radio-Frequency Plasma Torch for Atomic Emission and Atomic Absorption Spectroscopy, Spectrochim. Acta, Part B, 23, 503 (1968).

13. G. W. Dickinson and V. A. Fassel, Emission Spectrometric Detection of Elements at the Nanogram per Milliliter Level Using Inductively-Coupled Plasma Excitation, Anal. Chem. 41, 1021 (1969).

14. A. L. Davidson, J. R. Bethune, and R. M. Ajhor, 24th Pittsburg Conference on Anal. Chem. and Appl. Spec., Abstr., Paper No. 30, Cleveland, 1973.

15. A. L. Davidson, J. R. Bethune, and R. M. Ajhor, 25th Pittsburg Conference on Anal. Chem. and Appl. Spec., Abstr., Paper No. 147, Cleveland, 1974.

16. V. A. Fassel, Simultaneous or Sequential Determination of the Elements at all Concentration Levels-The Renaissance of an Old Approach, Anal. Chem. 51, 1290A (1979).

17. R. M. Barnes, CRC Crit. Rev. Anal. Chem. 7, 203-296 (1978).

18. W. J. Boyko, P. K. Keliher, and J. M. Malloy, Emission Spectroscopy, Anal. Chem. 52, 53R (1980).

19. I. Kleinmann and V. Svoboda, High Frequency Excitation of Independently Vaporized Samples in Emission Spectroscopy, Anal. Chem. 41, 1029 (1969).

20. D. J. Kalnicky, R. N. Kniseley, and V. A. Fassel, Inductively Coupled Plasma-Optical Emission Spectroscopy, Spectrochim. Acta, Part B, 30, 511 (1975).

21. G. F. Kirkbright and A. F. Ward, Atomic-Emission Spectroscopy with an Induction-Coupled High Frequency Plasma Source, Talanta 21, 1145 (1974).

22. K. W. Olson, W. J. Hass Jr., and V. A. Fassel, Multielement Detection Limits and Sample Nebulization Efficiencies of an Improved Ultrasonic Nebulizer and a Conventional Pneumatic Nebulizer in Inductively Coupled Plasma-Atomic Emission Spectroscopy, Anal. Chem. 49, 1413 (1977).

23. M. Margoshes and B. F. Scribner, The Plasma Jet as a Spectroscopic Source, Spectrochim. Acta 15, 138 (1959).

24. V. V. Korolev and E. E. Vainshtein, J. Anal. Chem. USSR 14, 731 (1959).

25. P. W. J. M. Boumans, Excitation of Spectra in Analytical Emission Spectroscopy, Part II, ed. by E. L. Grove, P. 204, Plenum Press, New York (1972).

26. C. D. Keirs and T. J. Vickers, dc Plasma Arcs for Elemental Analysis, Appl. Spec. 31, 273 (1977).

27. S. Greenfield, H. Mcb. Mc Greachin, and P. B. Smith, Plasma Emission Sources in Analytical Spectroscopy-I, Talanta 22, 1 (1975).

28. J. Reednick, A Unique Approach to Atomic Spectroscopy, American Laboratory, March, 53 (1979).

29. R. K. Skoegerboe, I. T. Urasa, and G. N. Coleman, Characterization of a dc Plasma as an Excitation Source for Multielement Analysis, Appl. Spec. 5, 500 (1976).

30. A. F. Ward, Inductively Coupled Argon Plasma Spectroscopy, American Laboratory, Nov., 79 (1978).

31. S. E. Valente and W. B. Skrenk, The Design and some Emission Characteristics of an Economical dc Arc Plasmajet Excitation Source for Solution Analysis, Appl. Spec. 24, 197 (1970).

32. J. E. Meinhard, Infor. Newsletter 2, 163 (1976).

33. R. S. Babington, Popular Science, May, 102 (1973).

34. R. S. Babington, U. S. Patent: 3,421,692; 3,421,699; 3,425,058; 3,425,059; and 3,504,859.

35. R. C. Fry and M. B. Denton, High Solids Sample Introduction for Flame Atomic Absorption Analysis, Anal. Chem. 49, 1413 (1977).

36. R. C. Fry and M. B. Denton, Characteristics of a High Solids Nebulizer for Flame Atomic Absorption Spectroscopy, Appl. Spec. 33, 393 (1979).

37. R. F. Suddendorf and K. W. Bayer, Nebulizer for Analysis of High Salt Content Samples with Inductively Coupled Plasma Emission Spectrometry, Anal. Chem. 50, 1769 (1978).

38. J. F. Wolcott and C. B. Sobel, A Simple Nebulizer for an Inductively Coupled Plasma System, Appl. Spec. 32, 591 (1978).

39. J. R. Garbarino and H. E. Taylor, A Babington-type Nebulizer for Use in the Analysis of Natural Water Samples by Inductively Coupled Plasma Spectrometry, Appl. Spec. 34, 584 (1980).

40. N. Mohammed, R. M. Brown Jr., and R. C. Fry, Slurry Atomization dc Plasma Emission Spectrometry and Laser Diffraction Studies of Aerosol Production and Transport, Appl. Spec. 35, 153 (1981).

41. P. W. J. M. Boumans and F. J. de Boer, Studies of an Inductively-Coupled High-Frequency Argon Plasma for Optical Emission Spectroscopy-II Compromise Conditions for Simultaneous Multielement Analysis, Spectrochim Acta, Part B, 30, 309 (1975).

42. J. D. Cobine, Gaseous Conductors, p. 294, Dover Publications, Inc., New York (1958).

43. C. H. Willis and H. W. Chandler, Introductory Electrical Engineering, p. 337-347, D. Van Nostrand Company, Inc., Princeton, New Jersey (1957).

44. P. W. J. M. Boumans, F. T. De Boer, F. J. Daham, H. Hoelzel, and A. Mejar, Spectrochim. Acta, Part B, 30, 449 (1975).

45. Improved Reproducibility, Plasma Line 1, 2 (1980).

46. S. A. Goldstein and J. P. Walters, Spectrochim. Acta, Part B, 31, Part I, 200, Part II, 295 (1976).

47. J. A. Dean and T. C. Rains, Flame Emission and Atomic Absorption Spectroscopy, Vol. 2 p. 332-336, Marcel Dekker, Inc., New York (1971).

48. R. K. Skoegerboe, I. T. Urasa, and G. N. Coleman, Characterization of a dc Plasma as an Excitation Source for Multielement Analysis, Anal. Chem., 30, 500 (1976).

49. J. D. Ingle, Jr., Notes on Basics Spectrometric Measurements, p. 67 (1978).

50. R. K. Winge, V. J. Peterson, and V. A. Fassel, Inductively Coupled Plasma: Prominent Lines, Applied Spec., 33, 206 (1979).

51. W. J. Dixon and F. J. Massey, Introduction to Statistical Analysis, p. 195, McGraw-Hill, Inc., San Francisco (1969).

52. R. K. Skogerboe and I. T. Urasa, Evaluation of the Analytical Capabilities of a dc Plasma-Echelle Spectrometer System, Applied Spec., 32, 527 (1978).

53. Vickers T. J. and J. D. Winefordner, Flame Spectrometry In: Analytical Emission Spectroscopy Part II, ed. by E. L. Grove, New York, p. 333 (1972).

54. V. A. Fassel and R. N. Kniseley, Inductively Coupled Plasma-Optical Emission Spectroscopy, Anal. Chem., 46, 1110A (1974).